Geological Society of America
Special Paper 371
2003

Magmatic and tectonic history of the Leech River Complex, Vancouver Island, British Columbia: Evidence for ridge-trench intersection and accretion of the Crescent Terrane

Wesley G. Groome*
Derek J. Thorkelson
Department of Earth Sciences, Simon Fraser University, Burnaby, British Columbia, V5A 1S6, Canada

Richard M. Friedman
James K. Mortensen
Department of Earth and Ocean Sciences, University of British Columbia, Vancouver, British Columbia, V6T 1Z4, Canada

Nick W.D. Massey
British Columbia Geological Survey Branch, Ministry of Energy and Mines, Victoria, British Columbia, V8W 9N3, Canada

Daniel D. Marshall
Department of Earth Sciences, Simon Fraser University, Burnaby, British Columbia, V5A 1S6, Canada

Paul W. Layer
Geophysical Institute, University of Alaska, Fairbanks, Alaska, 99775, USA

ABSTRACT

The Leech River Complex, part of the Pacific Rim Terrane, is a Cretaceous metasedimentary and metaigneous assemblage on southern Vancouver Island. The Leech River Complex is fault-bounded between the Eocene Metchosin Igneous Complex to the south (part of the Crescent Terrane) and the Paleozoic to Jurassic Wrangel Terrane to the north and provides critical information on the evolution of the central part of the western North American forearc in Cretaceous through Eocene time. Single detrital zircons from the metasedimentary component, known as the Leech River Schist, give U-Pb interpreted ages that range from Precambrian to ca. 103 Ma, indicating a varied source region and a probable Early Cretaceous depositional age. U-Pb geochronology and field investigations indicate at least two magmatic-metamorphic events in the Leech River Complex: one during the Late Cretaceous, and the other during the early Middle Eocene. The peraluminous Jordan River metagranodiorite, a fine-grained biotitic stock and related dikes intruded the Leech River Complex at ca. 88 Ma, during the older magmatic event. Metamorphic pressure-temperature conditions of 525–550 °C and 2–3 kbar are recorded in the contact aureole. The later event occurred during emplacement of the Walker Creek intrusions, a suite of peraluminous tonalite, trondjhemite, and granodiorite dikes that intruded the Complex at ca. 51 Ma and produced a similar metamorphic aureole. Both intrusive suites have

*Current address: Department of Geological Sciences, University of Maine, Orono, ME 04469, USA; wesley.groome@umit.maine.edu.

Groome, W.G., Thorkelson, D.J., Friedman, R.M., Mortensen, J.K., Massey, N.W.D., Marshall, D.D., and Layer, P.W., 2003, Magmatic and tectonic history of the Leech River Complex, Vancouver Island, British Columbia: Evidence for ridge-trench intersection and accretion of the Crescent Terrane, *in* Sisson, V.B., Roeske, S.M., and Pavlis, T.L., eds., Geology of a transpressional orogen developed during ridge-trench interaction along the North Pacific margin: Boulder, Colorado, Geological Society of America Special Paper 371, p. 327–353.

a variably developed schistosity that parallels foliation in the Leech River Schist, and may indicate emplacement during deformation. The Tripp Creek metabasite, a third intrusive unit with an N-MORB geochemical signature, is also interfoliated with the schist and may be the same age as one or both of the peraluminous intrusive suites. Taken together, these magmatic events may be rationalized as products of ridge subduction and slab window formation beneath the Leech River Complex, at the leading edge of the North American plate. Uprise of basaltic melts from the subducting ridge, and consequent anatexis of the forearc metasediments, accounts for the MORB-like and peraluminous intrusions, respectively.

^{40}Ar/^{39}Ar cooling ages for muscovite (ca. 45 Ma) and biotite (ca. 42.5 Ma) indicate rapid cooling of the Leech River Complex in the Middle Eocene. Cooling was probably related to exhumation and denudation of the Complex during underthrusting of the Crescent Terrane along the sinistral-oblique Leech River fault. The Leech River Complex is overlain by undeformed Oligocene Carmanah Group sediments.

Keywords: magmatism, tectonics, slab windows, geochronology, detrital mineral age, geochemistry, major elements, trace elements, Vancouver Island, British Columbia

INTRODUCTION

Forearc accretionary complexes are commonly characterized by low geothermal gradients and a lack of igneous activity (Gill, 1981; Best, 1982; Bucher and Frey, 1994). However, the entry of a spreading ridge into the subduction zone can increase the geothermal gradient, a situation commonly referred to as ridge subduction and slab window formation (Marshak and Karig, 1977; Delong et al., 1979; Dickinson and Snyder, 1979; Forsythe and Nelson, 1985; Sisson and Pavlis, 1993; Thorkelson, 1996). Where this occurs, the temperature of the forearc can be greatly elevated, leading to magmatism and high-temperature metamorphism (Delong et al., 1979; Sisson and Pavlis, 1993). The effects of ridge subduction farther inland, particularly below the arc, are more varied and may require geochemical data to delineate (e.g., Johnston and Thorkelson, 1997). Thus, the presence of magmatic activity within the forearc is arguably one of the key indicators of offshore plate configurations.

Early Tertiary forearc magmatism within the western Cordillera of North America took place in a belt extending from Alaska to Oregon. This belt can be subdivided into two segments, each with a distinct style and tectonic setting. Within a northern segment that extends from southeastern Alaska to southern Vancouver Island, forearc igneous rocks are hosted in accretionary complexes, including the Pacific Rim and Chugach terranes (Hill et al., 1981; Fairchild and Cowan, 1982; Rusmore and Cowan, 1985; Brandon, 1989; Barker et al., 1992; Sisson and Pavlis, 1993; Haeussler et al., 1995; Harris et al., 1996; Groome, 2000). These igneous rocks consist mainly of intermediate to felsic intrusions associated with high-temperature metamorphic assemblages (Hill et al., 1981; Fairchild and Cowan, 1982; Rusmore and Cowan, 1985; Brandon, 1989; Barker et al., 1992; Sisson and Pavlis, 1993; Groome, 2000). Subordinate felsic volcanics and mafic intrusions are present locally (Hill et al., 1981; Groome, 2000). This forearc magmatism has been interpreted to be the result of spreading-ridge subduction (Sisson and Pavlis, 1993; Groome et al., 2000). In the southern segment, which extends from southern Vancouver Island to southern Oregon, Early Tertiary forearc igneous rocks are represented by basaltic rocks of the Crescent Terrane. This terrane was interpreted by Duncan (1982) to be accreted seamounts, but more recent work suggests that it may have formed in a forearc rift basin, which was thrust beneath the continental margin in Eocene time (Wells et al., 1984; Massey, 1986; Babcock et al., 1992).

In this paper, we examine the forearc intrusions in the Leech River Complex, which is part of the Pacific Rim Terrane on southern Vancouver Island (Wheeler and McFeeley, 1991; Fig. 1). The main study area is located in the southeastern part of the Leech River Complex (Fig. 1). We report new results from field and petrographic studies, U-Pb and ^{40}Ar/^{39}Ar geochronology, and geochemistry, and define three intrusive suites ranging in age from Late Cretaceous to Middle Eocene. Variations in metamorphic grade are tied to thermal aureoles surrounding the plutons. Cooling ages for micas from the intrusions and their host rocks demonstrate rapid exhumation of the Leech River Complex, and are used to infer the timing of underthrusting of the Crescent Terrane. Subduction of the Kula-Farallon ridge may be linked to Eocene magmatism. Earlier subduction of an unknown spreading ridge is suggested as a possible cause of the Cretaceous igneous activity.

UNITS OF THE PACIFIC RIM TERRANE

The Pacific Rim Terrane is located on western and southern Vancouver Island. It is juxtaposed along faults with Wrangellia to the east and north, and the Crescent Terrane to the west and south. The Pacific Rim Terrane is broadly regarded as an accretionary complex, at least in part, and consists of three principal units: the Pacific Rim Complex, which extends along parts of western Vancouver Island (Brandon, 1989); the Pandora Peak unit, located mainly along southwestern Vancouver Island near Port Renfrew (Rusmore and Cowan, 1985); and the Leech River Complex

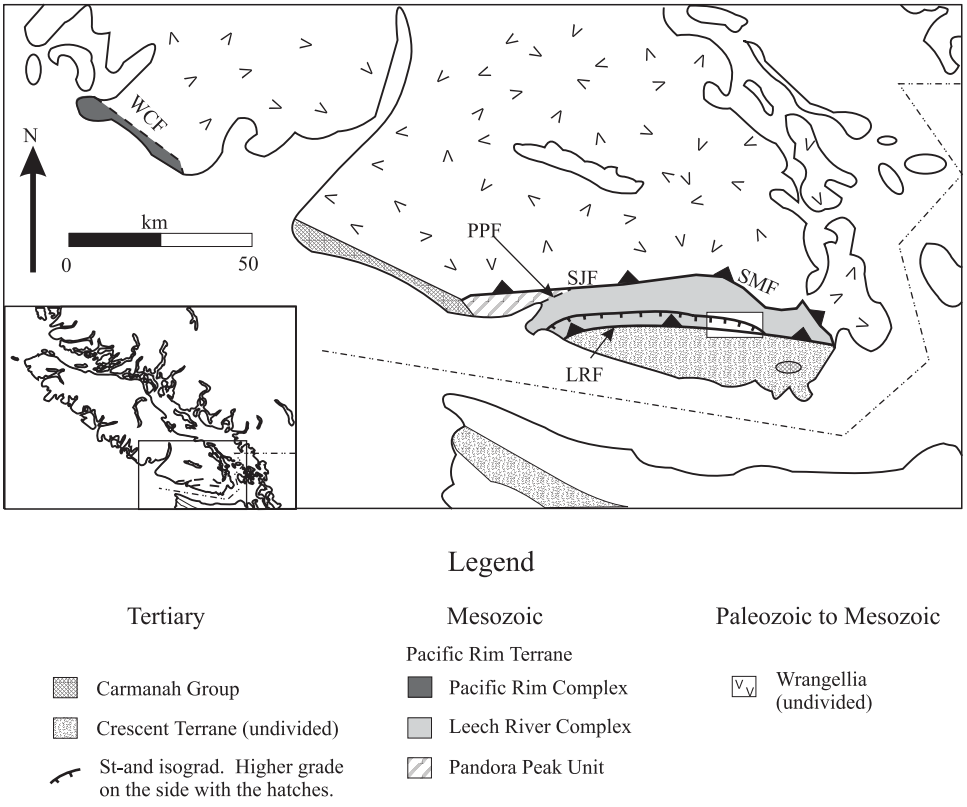

Figure 1. Simplified tectonic assemblage map of southern Vancouver Island (after Wheeler and McFeeley, 1991). Inset: Map of Vancouver Island region; box indicates the region of the main map in the figure. The staurolite isograd is from Read et al., 1991. LRF—Leech River fault; PPF—Pandora Peak fault; SJF—San Juan fault; SMF—Survey Mountain fault; WCF—Westcoast fault. The white box on the main figure outlines the region of Figure 2. St-and—Staurolite-andalusite isograds.

(Fairchild and Cowan, 1982), which extends across the southern end of the island. The basaltic Crescent Terrane is represented by the Metchosin Igneous Complex on the southern tip of Vancouver Island (Massey, 1986), and the Prometheus volcanics to the west of Vancouver Island beneath the Pacific Ocean (Shouldice, 1971). Wrangellia consists mainly of Lower Paleozoic to Mesozoic igneous and sedimentary rocks and was accreted to the continental margin in Jurassic to middle Cretaceous time. Wrangellia apparently served as a buttress against which the Pacific Rim and Crescent Terranes were accreted in Mesozoic to Eocene time. The timing and nature of the accretion of the Pacific Rim Terrane is not well understood and may involve considerable strike-slip faulting (Fairchild and Cowan, 1982; Rusmore and Cowan, 1985; Brandon et al., 1988). Accretion of the Crescent Terrane occurred in the Eocene (Massey, 1986).

The Leech River Complex, the Pandora Peak unit, and the Pacific Rim Complex are all included in the Pacific Rim Terrane (Wheeler and McFeeley, 1991) because of their common tectonic position and their typically disrupted to chaotic sedimentary character. The Leech River Complex differs from the other units by its characteristic foliation and generally higher metamorphic grade (Fairchild and Cowan, 1982; Rusmore and Cowan, 1985).

Pacific Rim Complex

The Pacific Rim Complex is located along the west coast of Vancouver Island. It consists of a Triassic arc sequence (Ucluth Formation) and an unconformably overlying olistostromal mélange (Brandon, 1989). The Ucluth Formation consists of volcanic and sedimentary strata of arc affinity (Brandon, 1989). The overlying olistostromal mélange unit consists of centimeter- to meter-scale angular blocks of chert, graywacke, argillite, and greenstone in a fine-grained matrix of mudstone to siltstone but does not display penetrative deformation (Brandon, 1989). The depositional age of the olistostromal unit is constrained by the presence of Jura-Cretaceous microfossils in the matrix sediments (Brandon, 1989).

Brandon (1989) showed that the Pacific Rim Complex was statically metamorphosed to prehnite-lawsonite grade and interpreted this metamorphism to be Cretaceous in age, based on $^{40}Ar/^{39}Ar$ geochronology on metamorphic minerals. The metamorphic conditions are suggestive of a subduction zone environment. However, Brandon (1989) suggested the rocks of the Pacific Rim Complex were deposited in a marginal basin within submarine debris flows, rather than within an accretionary wedge, based on the presence of blocks of Ucluth Formation greenstone within the mélange. In this scenario, the blueschist metamorphism would be post-deposition.

Pandora Peak Unit

The Pandora Peak unit is fault bounded between the Leech River Complex and Wrangellia near Port Renfrew along the Port Renfrew fault and the San Juan fault, respectively, and

is also in fault contact with Wrangellia near Victoria along the Trial Island fault. The Pandora Peak unit consists of black mudstone, terrigenous graywacke, radiolarian ribbon chert, green tuff, metabasaltic greenstone, pebbly mudstone, and local limestone blocks that were deposited during the Late Jurassic to Early Cretaceous (Rusmore and Cowan, 1985).

The Pandora Peak unit underwent blueschist facies metamorphism, with the assemblage of lawsonite-prehnite-calcite being characteristic (Rusmore and Cowan, 1985). The metamorphic assemblage present in the Pandora Peak unit indicates pressure-temperature conditions of about 3 kbar, 175–230 °C. (Rusmore and Cowan, 1985, and references therein).

Leech River Complex

The Leech River Complex is bounded to the north against the Pandora Peak unit and Wrangellia along the Port Renfrew, San Juan, and Survey Mountain faults, and to the south against the Metchosin Igneous Complex (Crescent Terrane) along the Leech River fault (Fairchild and Cowan, 1982; Rusmore and Cowan, 1985). The Leech River Complex consists of pelitic and arenaceous metasediments, and igneous rocks that have been variably metamorphosed and deformed (Fairchild and Cowan, 1982; Groome, 2000). In contrast to the Pandora Peak unit and the Pacific Rim Complex, rocks of the Leech River Complex are characterized by higher-temperature metamorphic assemblages and penetrative foliations.

Metamorphic grade in the Leech River Complex ranges from chlorite zone to staurolite-andalusite zone (Fairchild and Cowan, 1982; Rusmore and Cowan, 1985). Metamorphic grade generally increases towards the southern boundary of the Complex (Fairchild and Cowan, 1982; Rusmore and Cowan, 1985). In the eastern part of the Leech River Complex, increases in metamorphic grade are spatially and, apparently, genetically related to igneous intrusions (Groome et al., 1999). A causal relationship between igneous activity and increased metamorphic grade was also postulated for the western portion of the Complex by Rusmore and Cowan (1985). In the central portion of the Complex, which has not been studied in detail, the controls on metamorphism have not been documented.

Metapelitic rocks are the most abundant rock type in the Leech River Complex. They are typically brown- to black-weathering schist, with an assemblage of biotite-chlorite-white mica-plagioclase-quartz in the greenschist facies regions, and biotite-staurolite-andalusite-plagioclase-muscovite-quartz (± garnet, ± cordierite) in the amphibolite facies regions. The pelitic schist contains discontinuous lenses and patches of white-weathering metasiltite and fine-grained metasandstone; together, these metasediments constitute the Leech River Schist (Muller, 1983). The silty-sandy parts are generally 5–50 cm long and 1–5 cm thick, although some range up to 10 m long and 3 m thick. Their protoliths were probably sublithic to subarkosic arenites on the basis of modal mineralogy and textures in thin section. The metapelite and the coarser layers have been metamorphosed and deformed to such an extent that original sedimentary layering is not preserved. The highly discontinuous nature of the coarse layers is partly due to boudinage and other processes of post-lithification deformation, but a fundamental cause of their ragged shapes and chaotic distribution may be largely synsedimentary in origin, possibly the result of slumping during olistostrome formation. Very similar textures are present in the olistostromal unit of the Pacific Rim Complex, which was not penetratively deformed after lithification (Brandon, 1989).

Metaigneous rocks are also present in the Leech River Complex. Foliated and metamorphosed basaltic layers with small (~1 mm) but conspicuous porphyroclasts of altered plagioclase in the eastern part of the Complex were named the Survey Mountain volcanics by Fairchild (1979). In our study, these rocks were briefly inspected and textures diagnostic of lava or tuffaceous rock were not encountered. Therefore these rocks could be intrusive. If so, they could either be a lower-grade manifestation of the Tripp Creek metabasite or could form a fourth intrusive unit unrelated to the other intrusive units of the Leech River Complex.

INTRUSIVE ROCKS OF THE LEECH RIVER COMPLEX

Three intrusive units are present in the area of detailed study (Fig. 2): the Walker Creek intrusions, the Jordan River metagranodiorite, and the Tripp Creek metabasite. The Walker Creek intrusions are the most widespread intrusive rocks in the study area. They form a tonalite-trondjhemite-granodiorite suite of dikes and sills ranging in size from a few centimeters wide to several meters wide. The Jordan River metagranodiorite crops out as a large stock and several smaller intrusions. The Tripp Creek metabasite consists of several layers of actinolite-rich schist and minor metagabbro. All three intrusive units contain a penetrative foliation. New age determinations, given below, indicate that the Jordan River metagranodiorite is Late Cretaceous, and the Walker Creek intrusions are Eocene. The Tripp Creek metabasite was not dated but is likely to be late Early Cretaceous to Eocene on the basis of similar fabrics and field relations.

Geochemical analyses were obtained for all of the intrusive suites. Samples submitted for analysis were devoid of weathering rinds and were ground in agate. Major oxide analyses were determined by XRF on fused disks at X-Ray Assay Labs, and trace element analyses were carried out by ICP-MS at the University of Saskatchewan. Precision of the major oxides, provided by the laboratory, ranges from 1% to 2% of the reported values. For each trace element, precision was evaluated according to the determination limit provided by the laboratory, and a percentage of the reported element abundance as determined graphically on duplicate analyses (Groome, 2000). Analytical accuracy was evaluated using two CANMET reference materials, MRG-1 and SY-2. The reported values of these standards, when compared to the expected (accepted) abundances, lie within the determined levels of analytical precision.

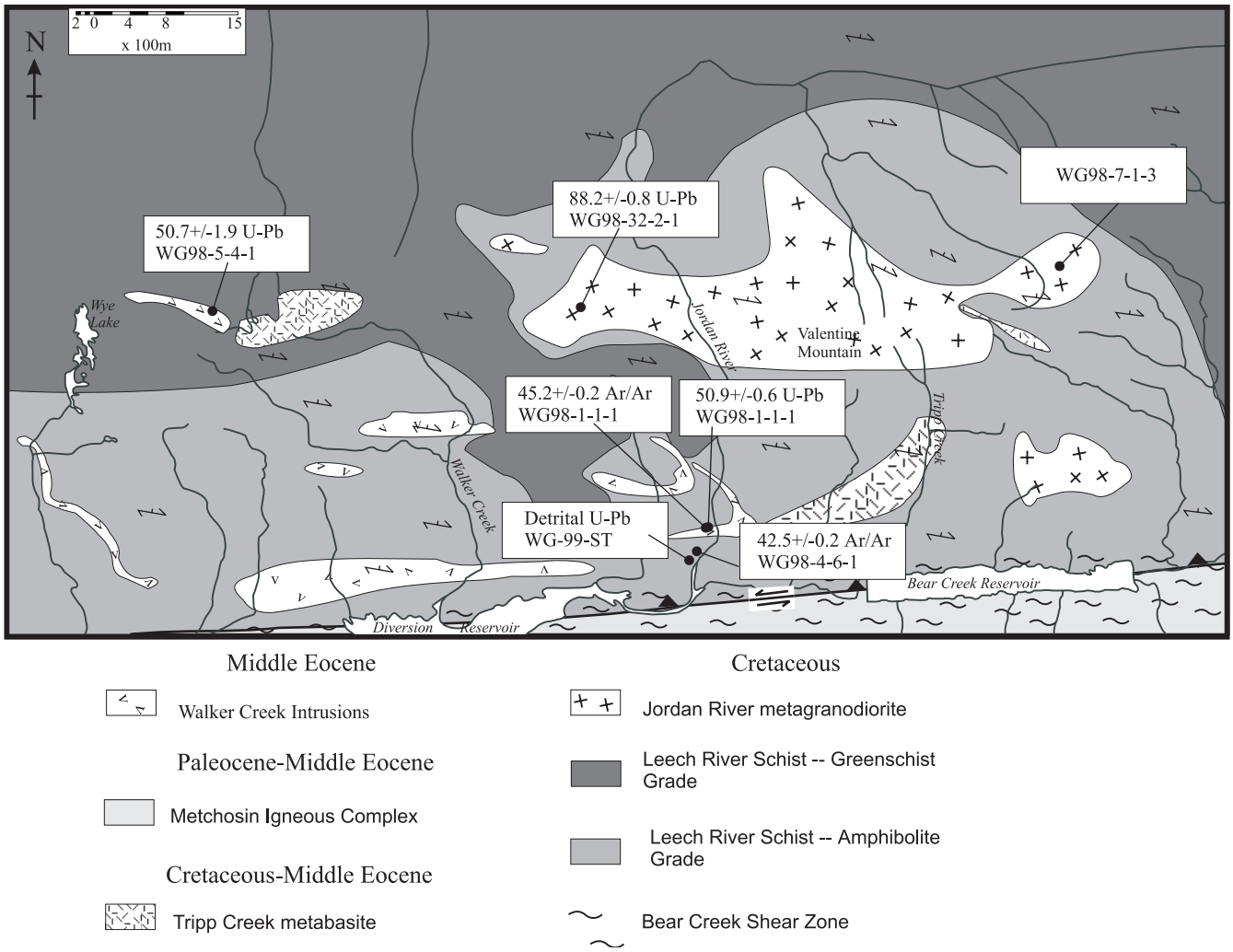

Figure 2. Simplified geologic map of the Jordan River region of the Leech River Complex (modified from Groome, 2000). Sample locations of dated rocks are shown. Foliations are representative and generalized.

Jordan River Metagranodiorite

The Jordan River metagranodiorite comprises a homogenous 6 km long by 2 km wide by 500 m thick stock and approximately ten smaller stocks and dikes. It is a mesocratic biotite ± hornblende granodiorite that is interfoliated with the Leech River Schist along the margins and less deformed towards the interior. The smaller comagmatic dikes and stocks that were found in the study area are interfoliated with the Leech River Schist. These dikes are interpreted to be comagmatic with the Jordan River metagranodiorite based on compositional and structural similarities. Both the main stock and the smaller dikes contain xenoliths of Leech River Schist that preserve penetrative fabrics with orientations independent of the fabric in the intrusion.

In thin section, the Jordan River metagranodiorite has few features preserved that are easily recognizable as primary in origin. Most of the samples appear to have been recrystallized, as indicated by the presence of overgrowths and sutures on most of the grains. The groundmass crystals have a strong preferential orientation, while the larger grains appear to have been rolled during deformation, as indicated by asymmetric pressure shadows. Some plagioclase phenocrysts/porphyroblasts have pressure shadows developed around them, indicative of deformation partitioning during recrystallization. The foliation is defined by the preferential orientation of biotite and of multigrain quartz stringers.

Plagioclase (~An_{30}) is the most abundant rock-forming mineral in the Jordan River metagranodiorite. It constitutes up to 40% of the mode, and is distributed throughout the groundmass and as a phenocryst/porphyroblast phase in most samples. The plagioclase is variably altered to fine-grained clay and muscovite. Quartz and alkali-feldspar are present primarily as groundmass phases in thin section. Some alkali-feldspar crystals have perthitic exsolution present. A few crystals of quartz

have a myrmekite texture developed with plagioclase, possibly indicative of simultaneous growth of the two phases.

The primary ferro-magnesian silicate in the Jordan River metagranodiorite is biotite, which generally occurs as well-developed crystals that help to define a foliation. Some of the biotite crystals are pseudomorphed by retrograde chlorite. Hornblende, also present in the Jordan River metagranodiorite, is typically euhedral and partially altered to biotite. In the samples that have no hornblende, it appears that the biotite is primary, as the crystals do not display the morphology of hornblende, and no relict hornblende is present in the cores of the biotite crystals.

Accessory minerals in the Jordan River metagranodiorite include apatite, zircon, titanite, hematite, and other opaques. The Jordan River metagranodiorite is also locally mineralized with chalcopyrite, pyrite, and arsenopyrite. Where observed, this mineralization is disseminated and is spatially associated with alteration zones. These alteration zones are characterized by a reddish iron-oxide staining and a friable character. Abundant quartz veins are also associated with the mineralized zones, implying that the mineralization is the result of post-crystallization hydrothermal activity.

The chemical composition of the metagranodiorite is quite uniform, as indicated by three analyses, two from the main stock and one from a smaller stock. Major element concentrations and CIPW normative mineralogy (Table 1) indicate that the metagranodiorite is slightly peraluminous, sodic, and quartz and hypersthene normative. Trace element abundances normalized to normal mid-ocean ridge basalt (N-MORB) are displayed in Figure 3A. All of these patterns resemble modern continental arcs, with high alkali and alkaline earth concentrations, and relative depletions in Nb and Ta (Fig. 3E). Two samples from the Leech River Schist, shown on Figure 3D, are remarkably similar in chemical composition to the Jordan River intrusions. On discriminant diagrams of Pearce et al. (1984), the Jordan River metagranodiorite samples plot as volcanic arc granitoids (VAG) (Fig. 4).

Tripp Creek Metabasite

The Tripp Creek metabasite comprises at least five lens-like layers up to 20 m thick that are interfoliated with the Leech River Schist, some of which is unusually biotite-rich. It also occurs within cliff faces along the banks of Tripp Creek, as variably foliated, fine- to medium-grained garnet-quartz-plagioclase-actinolite metagabbro that trends into outcrops of fine-grained actinolite-rich schist (Fig. 5). Original contact relations between the Tripp Creek metabasite and the Leech River Schist are obscured by deformation and metamorphism. However, the local igneous texture, and a xenolith of pelitic schist within the metabasite, suggests that the metabasite is intrusive. At some localities, the metabasite is spatially associated with the Walker Creek intrusions. This relation is particularly well expressed along Tripp Creek, where the metabasite crops out within a swarm of closely spaced Walker Creek intrusions. The metabasite is mainly com-

TABLE 1. WHOLE ROCK GEOCHEMISTRY AND CIPW NORMATIVE MINERALOGY

Sample:	98-15-1-1B	98-33-3-2B	98-14-4-1B	98-5-4-2B	98-12-5-1B	98-10-2-2B	98-12-1-1B	98-1-1-1B	98-5-2-3B	98-9-3-2B	98-5-5-3B	99-1-1-1B	99-2-1-1B	98-7-2-2B	98-4-6-1B	Detection
Unit:	KJR	KJR	KJR	eTWC	eTWC	eTWC	eTWC	eTWC	eTWC	eTWC	KeTTC	KeTTC	KeTTC	KLRa	KLRg	Limit
Rock type:	GD	GD	GD	GD	GD	TO	TO	TR	TO	TR	MB	MB	MB	ST	BT	
Northing:	5375326	5374264	5373507	5375781	5372755	5374006	5373016	5373871	5376057	5374291	5375628	5375221	5374232	5375448	5373038	%
Easting:	10430282	10434487	10430772	10425690	10429924	10429687	10428154	10430861	10424497	10430780	10425858	10428031	10431003	10475448	10429581	
Major oxides																
Wt%																
SiO_2	70.91	69.86	70.03	63.10	71.39	70.35	75.79	75.60	75.70	76.98	49.25	46.20	55.10	62.91	65.27	0.01
TiO_2	0.49	0.51	0.48	0.80	0.21	0.27	0.05	0.03	0.01	0.01	1.53	0.91	0.74	0.84	0.74	0.01
Al_2O_3	14.54	15.09	15.02	16.23	16.43	16.95	14.32	14.87	15.18	15.34	14.68	20.30	14.90	19.51	17.56	0.01
Fe_2O_3	3.87	4.10	3.77	5.89	1.55	2.70	1.09	1.32	0.81	0.68	12.30	10.00	9.89	8.05	5.79	0.01
MnO	0.05	0.06	0.06	0.08	0.02	0.04	0.02	0.03	0.03	0.04	0.19	0.15	0.14	0.10	0.10	0.01
MgO	1.73	1.99	1.81	3.96	0.84	0.62	0.14	0.07	0.04	0.03	9.26	7.35	7.52	3.15	2.55	0.01
CaO	3.18	3.15	3.40	4.92	2.80	3.10	1.34	1.52	1.04	0.67	11.52	13.66	8.73	1.21	2.97	0.01
Na_2O	3.96	3.61	3.85	4.00	6.05	4.59	4.40	4.41	4.84	4.15	2.01	2.10	2.50	1.27	2.99	0.01
K_2O	1.50	1.87	1.79	1.36	0.79	1.48	2.94	2.17	2.37	2.07	0.14	0.23	0.56	3.30	2.21	0.01
P_2O_5	0.12	0.11	0.12	0.20	0.06	0.13	0.03	0.07	0.07	0.11	0.12	0.08	0.13	0.16	0.18	0.01
LOI	0.50	0.90	0.35	0.40	0.65	0.65	0.20	0.70	0.65	0.95	0.25	0.25	1.80	1.80	1.80	
SUM	100.35	100.36	100.33	100.55	100.14	100.23	100.11	100.10	100.08	100.06	101.01	100.98	100.21	100.49	100.38	

Note: Rock type abbreviations: GD—granodiorite, TO—tonalite, TR—trondjhemite, ST—staurolite schist, BT—biotite schist, MB—metabasite. Data labels are used on all discriminant diagrams. KJR—Jordan River metagranodiorite; eTWC—Walker Creek intrusions; KLRa—Leech River Schist, amphibolite facies; KLRg—Leech River Schist, greenschist facies; KeTTC—Tripp Creek metabasite.

(continued)

TABLE 1. WHOLE ROCK GEOCHEMISTRY AND CIPW NORMATIVE MINERALOGY (continued)

Sample:	98-15-1-1B	98-33-3-2B	98-14-4-1B	98-5-4-2B	98-12-5-1B	98-10-2-2B	98-12-1-1B	98-1-1-1B	98-5-2-3B
Unit:	KJR	KJR	KJR	eTWC	eTWC	eTWC	eTWC	eTWC	eTWC
Rock type:	GD	GD	GD	GD	GD	TO	TO	TR	TO
Trace elements (ppm)									
Cs	2	2.4	1.7	4.3	1.3	2.3	2.8	2.3	0.82
Ba	680	700	630	480	1300	480	860	570	780
Rb	48	51	48	42	19	41	90	35	73
Th	5.5	4.5	4.2	4.1	1.4	3.5	4.2	2.4	2.2
Pb	10	12	9.8	18	13	12	28	9.1	21
U	1.5	1.5	1.1	2.3	0.47	1.1	1.3	1.2	2.4
K*	12000	16000	15000	11000	6600	12000	24000	18000	20000
Nb	6.7	7	6.7	10	1.5	8.4	11	6.6	9.1
Ta	0.54	0.43	0.45	0.57	0.12	0.63	1.2	0.55	1
La	21	18	18	20	4.6	21	13	13	9.2
Ce	40	35	35	38	8.8	37	24	23	18
Sr	620	350	340	690	950	740	130	350	220
Pr	4.8	4.2	4.2	4.6	1.1	4	2.8	2.5	2.1
Nd	19	16	16	18	4.4	14	11	8.5	7.7
P**	430	210	430	800	200	460	73	200	170
Zr	160	130	120	160	82	190	60	41	33
Hf	4	3.6	3.2	4.1	2.3	4.5	2.3	1.8	1.8
Sm	3.5	3.2	3.2	3.6	0.84	2.5	2.8	1.6	2.1
Eu	0.86	0.83	0.86	1.2	0.31	0.81	0.42	0.41	0.32
Gd	3	2.8	2.8	3.1	0.73	1.8	2.3	1.3	1.8
Tb	0.42	0.38	0.39	0.43	0.09	0.23	0.26	0.16	0.21
Ti***	2900	2500	2900	4600	1300	1600	280	140	43
Dy	2.5	2.3	2.4	2.5	0.48	1.3	1.1	0.87	0.84
Ho	0.51	0.45	0.46	0.45	0.09	0.23	0.14	0.15	0.1
Er	1.5	1.3	1.4	1.2	0.24	0.67	0.29	0.38	0.2
Tm	0.23	0.2	0.19	0.16	0.03	0.09	0.04	0.05	0.03
Y	15	13	13	13	4.1	8	5.2	5.6	4.2
Yb	1.5	1.3	1.3	1.1	0.19	0.62	0.22	0.31	0.12
Lu	0.21	0.18	0.2	0.14	0.03	0.1	0.03	0.03	0.01
V	83	84	84	130	29	4.6	3.1	0.39	0.91
Sc	10	11	10	13	3.8	3.1	1.4	0.83	1.2
Cr	50	37	52	85	26	5.5	11	8.9	20
Ni	18	14	16	82	5.7	2	1.4	0.64	1.4

*K = K_2O * 8300
**P = P_2O_5 * 4360
***Ti = TiO_2 * 6000
**P = P_2O_5 * 4360

(continued)

posed of green, fine-grained, strongly foliated, garnet-quartz-plagioclase-actinolite schist. The foliation is mainly defined by actinolite but is accentuated by preferred orientations of quartz and plagioclase. Garnet typically occupies <2% of the rock, and tends to be restricted to thin (grain-wide) layers.

Three samples of metabasite were analyzed for major and trace elements. On the basis of major elements (Table 1), the unit is basaltic, hypersthene-normative, and metaluminous, with magnesium numbers {100[Mg/(Mg + Fe)]} of approximately 63. Trace element profiles of the samples show nearly flat profiles on an N-MORB-normalized diagram (Fig. 3B). Of particular note is sample WG99-1-1-1B, which is a relatively undeformed metagabbro. The pattern of this sample is quite flat, with moderate enrichments in Cs, Ba, K and Sr, all of which are relatively mobile and may have been enriched during metamorphism. Variations in the profiles of the two other samples can be attributed to the nature of the samples collected. Both samples are actinolite schists and are deformed and metamorphosed to such an extent that original igneous textures are obliterated. The higher degree of deformation and more pervasive metamorphism could have resulted in increased mobility of incompatible elements.

Walker Creek Intrusions

The Walker Creek intrusions consist of a tonalite-trondhjemite-granodiorite suite of at least 100 tabular and lens-like

TABLE 1. WHOLE ROCK GEOCHEMISTRY AND CIPW NORMATIVE MINERALOGY (continued)

Sample:	98-9-3-2B	98-5-5-3B	99-1-1-1B	99-2-1-1B	98-7-2-2B	98-4-6-1B	Detection	ppm	Uncertainty
Unit:	eTWC	KeTTC	KeTTC	KeTTC	KLRa	KLRg	limit		
Rock type:	TR	MB	MB	MB	ST	BT	%		
Trace elements (ppm)									
Cs	0.83	0.04	0.04	1.1	1.8	3.1		0.03	10
Ba	720	23	25	270	820	700		0.17	10
Rb	47	0.78	1.1	17	63	63		0.03	10
Th	1.1	0.37	0.1	2.2	9.1	7.2		0.01	15
Pb	15	3.6	-1	5	14	16		0.05	25
U	1.4	0.13	0.08	1.1	1.9	1.5		0.03	10
K*	17000	1200	1900	4600	27000	18000		83	5
Nb	7.7	4.1	1.9	7.3	12	12		0.50	20
Ta	0.97	0.28	0.13	0.34	0.74	0.74		0.03	10
La	4.3	4.6	2	10	21	22		0.01	10
Ce	8.8	13	6	23	45	45		0.03	5
Sr	130	330	220	290	320	330		0.50	20
Pr	1.1	2	1.1	2.7	5.2	5.4		0.20	10
Nd	3.9	10	5.8	12	20	22		0.03	10
P**	340	490	350	570	560	650		43	5
Zr	30	86	50	110	130	140		0.11	10
Hf	1.7	2.5	1.4	2.8	3.6	3.8		0.10	15
Sm	1.3	3.3	2.1	2.7	4.1	4.5		0.03	10
Eu	0.1	1.1	0.9	0.85	0.97	1.2		0.03	10
Gd	1.6	4	3	2.8	3.9	4.2		0.03	10
Tb	0.26	0.68	0.55	0.47	0.6	0.6		0.03	15
Ti***	31	8800	5500	4400	5000	4800		4.00	10
Dy	1.5	4.3	3.7	3	3.6	3.6		0.03	10
Ho	0.24	0.86	0.76	0.63	0.75	0.7		0.10	20
Er	0.59	2.5	2.3	1.7	2.2	2		0.10	20
Tm	0.07	0.34	0.35	0.26	0.34	0.29		0.03	20
Y	8.1	22	22	18	21	19		0.01	15
Yb	0.43	2.2	2.2	1.7	2.1	1.9		0.10	25
Lu	0.04	0.3	0.36	0.26	0.33	0.29		0.01	10
V	0.34	330	220	170	260	210		0.33	20
Sc	0.69	40	32	25	12	16		0.40	15
Cr	5.4	410	320	410	120	120		1	20
Ni	0.89	180	94	110	57	28		0.10	10

*K = K_2O * 8300
**P = P_2O_5 * 4360
***Ti = TiO_2 * 6000
**P = P_2O_5 * 4360

(continued)

bodies that vary in width from a few cm to several m. Almost all are interfoliated with the enclosing Leech River Schist. The foliation in the intrusions is generally a fine-grained schistosity defined by muscovite and biotite. A few of the intrusions are weakly deformed to undeformed, indicating that magmatism may have outlasted the development of foliation. Many of the intrusions are isolated and separated from one another by tens to hundreds of meters. Others are clustered together, locally forming sheeted dike swarms up to 4 km long and 250 m wide (Fig. 6). The largest single dike is 50 m thick and 1 km long, and belongs to a swarm that crops out along Walker Creek. Many of the Walker Creek intrusions contain abundant metapelitic xenoliths that range from well-preserved clasts with detailed textures to partially digested, featureless ones with indistinct margins (Fig. 7). A thermal aureole similar to the one enclosing the Jordan River metagranodiorite surrounds the areas of concentrated Walker Creek magmatism.

In thin section, Walker Creek intrusions are commonly equigranular, and locally weakly plagioclase-phyric. Groundmass grain size ranges from 0.1 mm to 15 mm, averaging approximately 0.5 to 1.5 mm. Pressure shadows are developed around phenocrysts in some samples, indicative of sub-solidus deformation of these intrusions. A fabric is defined in several samples by the orientation of these pressure shadows, the preferential

TABLE 1. WHOLE ROCK GEOCHEMISTRY AND CIPW NORMATIVE MINERALOGY (continued)

Sample:	98-15-1-1B	98-33-3-2B	98-14-4-1B	98-5-4-2B	98-12-5-1B	98-10-2-2B	98-12-1-1B	98-1-1-1B	98-5-2-3B	98-9-3-2B	98-5-5-3B	99-1-1-1B	99-2-1-1B
Unit:	KJR	KJR	KJR	eTWC	eTWC	eTWC	eTWC	eTWC	eTWC	eTWC	KeTTC	KeTTC	KeTTC
Rock type:	GD	GD	GD	GD	GD	TO	TO	TR	TO	TR	MB	MB	MB
Fe_2O_3/FeO	0.20	0.20	0.20	0.20	0.20	0.20	0.20	0.20	0.20	0.20	0.20	0.20	0.20
Wt% Ap	0.28	0.26	0.28	0.47	0.14	0.31	0.07	0.17	0.16	0.26	0.28	0.19	0.30
Wt% Il	0.93	0.98	0.92	1.52	0.39	0.51	0.09	0.05	0.02	0.01	2.90	1.73	1.42
Wt% Or	8.88	11.06	10.54	8.03	4.67	8.75	17.38	12.84	14.01	12.21	0.84	1.36	3.33
Wt% Ab	33.47	30.55	32.51	33.82	51.19	38.79	37.16	37.29	40.88	35.06	16.95	14.07	21.28
Wt% An	14.99	14.89	16.07	22.27	13.49	14.50	6.46	7.06	4.68	2.58	30.55	45.17	27.95
Wt% C	0.90	1.65	0.86	0.00	0.67	2.48	1.53	2.67	2.94	5.33	0.00	0.00	0.00
Wt% Mt	0.87	0.92	0.85	1.32	0.35	0.61	0.24	0.30	0.18	0.15	2.77	2.21	2.21
Wt% Di	0.00	0.00	0.00	0.66	0.00	0.00	0.00	0.00	0.00	0.00	20.97	17.93	12.08
Wt% Hy	8.56	9.51	8.68	15.91	3.79	4.66	1.70	1.92	1.18	1.01	19.75	0.00	24.65
Wt% Ol	0.00	0.00	0.00	0.00	0.00	0.00	0.00	0.00	0.00	0.00	4.98	15.36	0.00
Wt %Q	31.13	30.20	29.29	16.00	25.32	29.39	35.37	37.70	35.95	43.39	0.00	0.00	6.78
Wt% Ne	0.00	0.00	0.00	0.00	0.00	0.00	0.00	0.00	0.00	0.00	0.00	1.98	0.00
SiO2 Def.	0.00	0.00	0.00	0.00	0.00	0.00	0.00	0.00	0.00	0.00	0.00	0.00	0.00
MIN SUM	100.00	100.00	100.00	100.00	100.00	100.00	100.00	100.00	100.00	100.00	100.00	100.00	100.00
Mol% Al_2O_3	0.14	0.15	0.15	0.16	0.16	0.17	0.14	0.15	0.15	0.15	0.14	0.20	0.15
Mol% Na_2O	0.06	0.06	0.06	0.06	0.10	0.07	0.07	0.07	0.08	0.07	0.03	0.03	0.04
Mol% K_2O	0.02	0.02	0.02	0.01	0.01	0.02	0.03	0.02	0.03	0.02	0.00	0.00	0.01
Mol% CaO	0.06	0.06	0.06	0.09	0.05	0.06	0.02	0.03	0.02	0.01	0.21	0.24	0.16
Mol% A/CNK	1.04	1.10	1.04	0.95	1.03	1.15	1.11	1.20	1.22	1.49	0.60	0.71	0.72
Mol% A/NK	1.79	1.89	1.82	2.01	1.52	1.85	1.37	1.55	1.44	1.69	4.24	5.48	3.16
Alumina class	Per	Per	Per	Met	Per	Per	Per	Per	Per	Per	Met	Met	Met
Rock Mg#	50.81	52.90	52.46	60.93	55.59	34.56	23.09	11.03	10.35	9.35	63.31	63.20	63.99
Silicate Min Mg#	56.96	58.90	58.51	66.96	61.83	39.34	25.32	11.92	10.86	9.56	68.67	67.62	67.89
Na_2O - K_2O<>2	Sod	Pot	Sod	Sod	Sod	Sod	Pot	Sod	Sod	Sod	Pot	Pot	Pot
Plag Ab%	70.34	68.54	68.24	61.71	80.12	73.97	85.93	84.87	90.28	93.53	37.07	29.40	44.69
Plag An%	29.66	31.46	31.76	38.29	19.88	26.03	14.07	15.13	9.72	6.47	62.93	70.60	55.31

Note: Normative minerals: Ab—albite; Il—ilmenite; An—anorthite; Mt—magnetite; Ap—apatite; Ne—nepheline; C—corundum; Ol—olivine; Di—diopside; Or—orthoclase; Hy—hypersthene; Q—quartz. Petrologic data: A/CNK = $Al_2O_3/(CaO + Na_2O + K_2O)$; A/NK = $Al_2O_3/(Na_2O + K_2O)$; Per = peraluminous (A/CNK > 1); Met = metaluminous (A/CNK < 1); Mg# = MgO/(MgO + FeO); Pot = potassic ($Na_2O – K_2O > 2$); Sod = sodic ($Na_2O – K_2O < 2$).

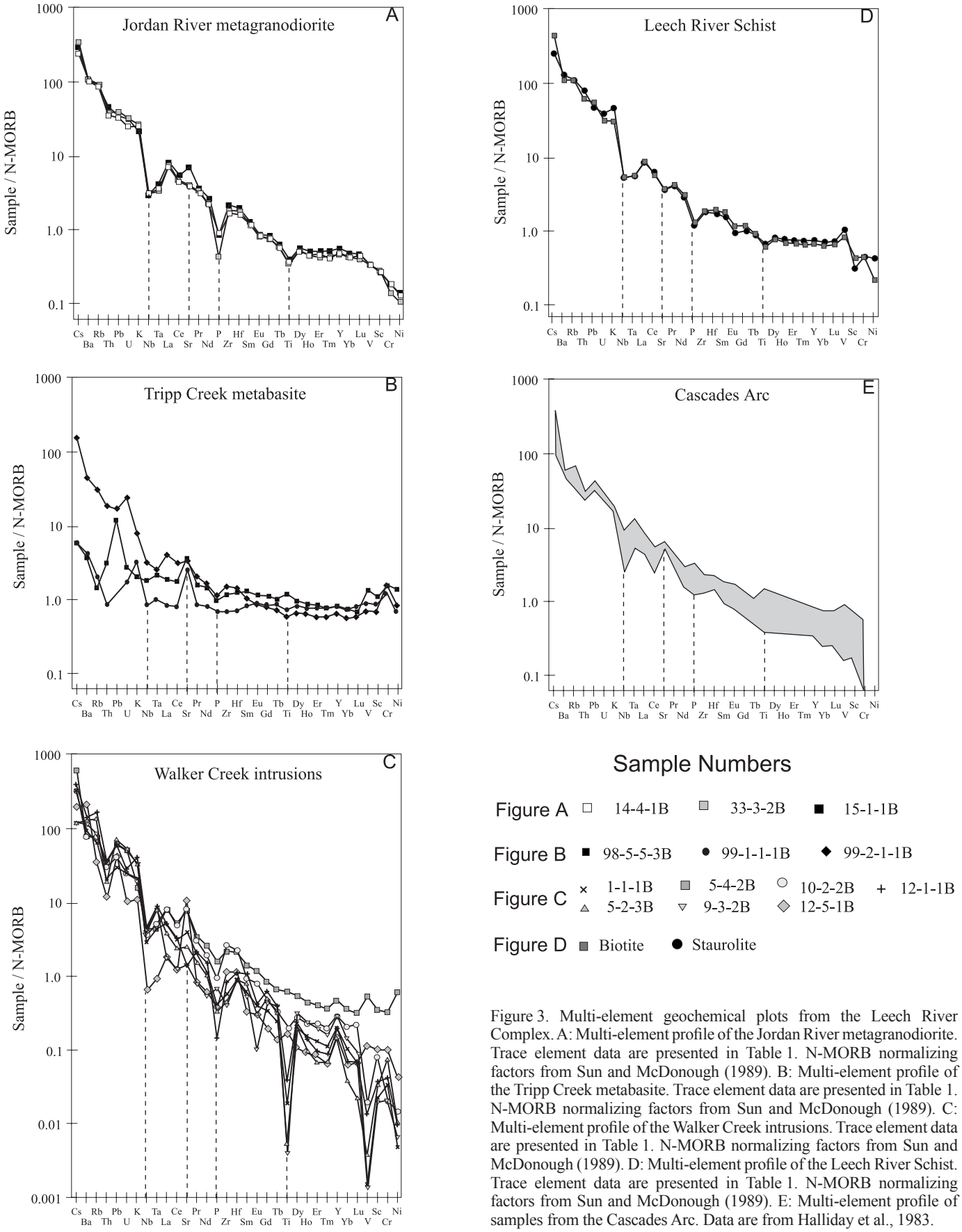

Figure 3. Multi-element geochemical plots from the Leech River Complex. A: Multi-element profile of the Jordan River metagranodiorite. Trace element data are presented in Table 1. N-MORB normalizing factors from Sun and McDonough (1989). B: Multi-element profile of the Tripp Creek metabasite. Trace element data are presented in Table 1. N-MORB normalizing factors from Sun and McDonough (1989). C: Multi-element profile of the Walker Creek intrusions. Trace element data are presented in Table 1. N-MORB normalizing factors from Sun and McDonough (1989). D: Multi-element profile of the Leech River Schist. Trace element data are presented in Table 1. N-MORB normalizing factors from Sun and McDonough (1989). E: Multi-element profile of samples from the Cascades Arc. Data are from Halliday et al., 1983.

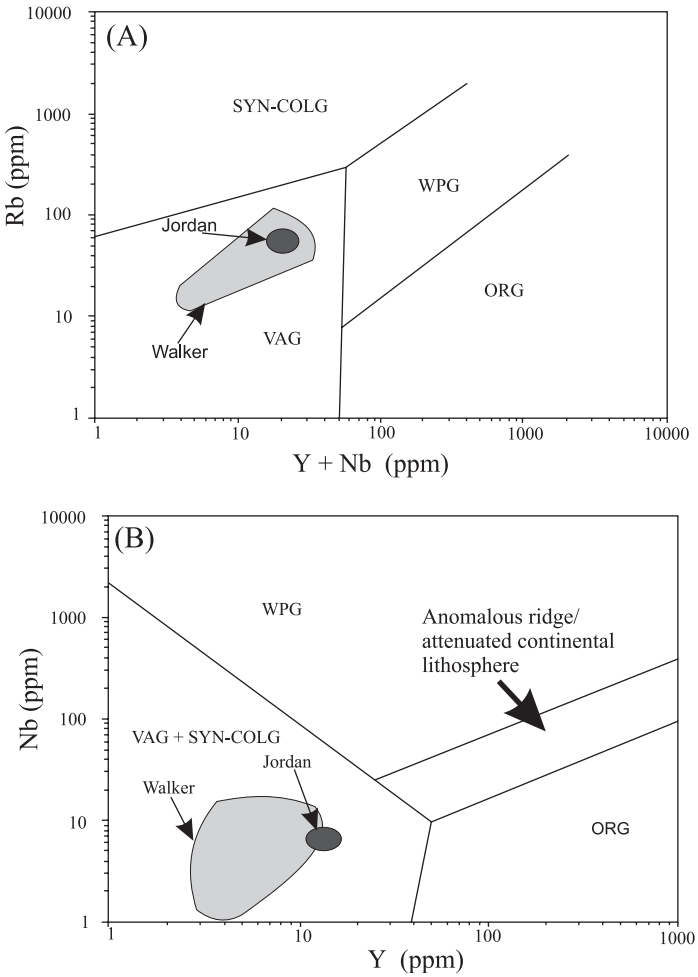

Figure 4. Tectonic affinity diagrams for granitoids from Pearce et al. (1984) with the Jordan River metagranodiorite and the Walker Creek intrusions displayed. A: Rb vs. Y + Nb. B: Nb vs. Y. SYN-COLG—syn-collisional granite, WPG—within plate granite, VAG—volcanic arc granite, ORG—orogenic granite.

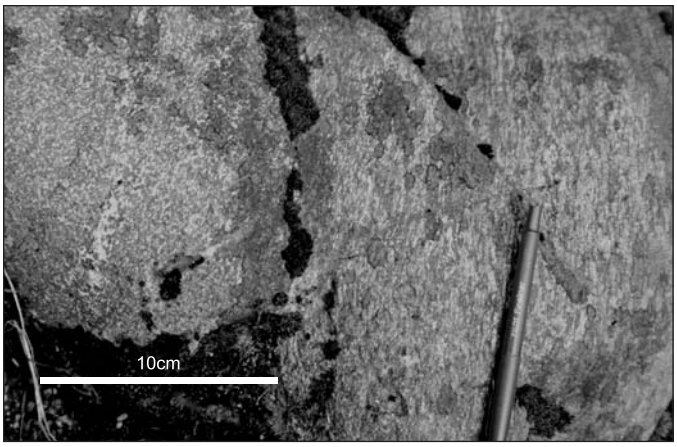

Figure 5. Photograph of gabbroic and schistose textures within the Tripp Creek metabasite.

Figure 6. Photograph of Walker Creek intrusions in outcrop. Only the three largest dikes in the outcrop are outlined. WCI—Walker Creek intrusion.

orientation of mica, and by a weak preferential orientation of multi-domainal quartz and plagioclase.

Plagioclase feldspar, alkali feldspar, and quartz together constitute up to 90% by volume of the Walker Creek intrusions. Plagioclase (An_5–An_{30}) content in the Walker Creek intrusions contributes between 40% and 60% by volume. Primary alkali-feldspar ranges from 5% to 30%; secondary alkali-feldspar constitutes up to ~15%; and quartz ranges from 15% to 35%. Primary (igneous) alkali-feldspar was recognized optically by the presence of exsolution lamellae as well as textural relationships with other igneous minerals. The primary alkali-feldspars are dispersed throughout the groundmass of many samples and are generally more euhedral than the secondary feldspars. Secondary (alteration) alkali feldspar was recognized optically based on the lack of exsolution lamellae as well as textural relationships with the igneous minerals. Secondary alkali-feldspar commonly

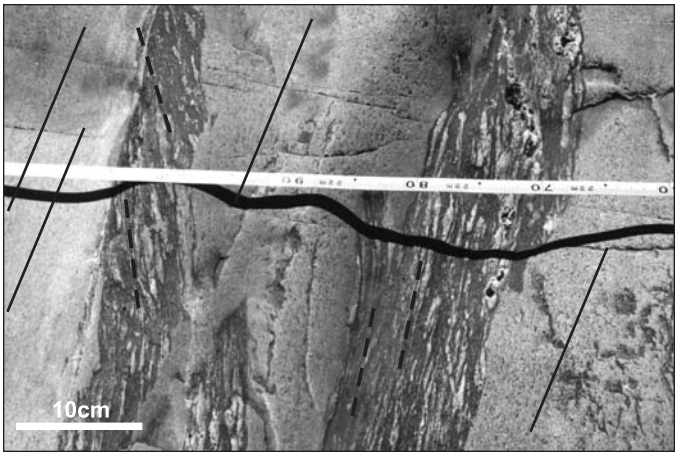

Figure 7. Photograph of xenoliths of Leech River Schist within the Walker Creek intrusions. Solid lines represent the fabric in the intrusions, while the dashed lines represent the fabric in the xenoliths.

occurs in small veinlets that fill fractures in the samples. In thin section, most quartz occurs as multi-domainal masses, which appear to have been single crystals prior to deformation. Quartz is also dispersed throughout the groundmass of most samples.

The main ferro-magnesian silicate in the Walker Creek intrusions is biotite, which makes up approximately 1% to 20%. In some samples, biotite is partially pseudomorphed by chlorite. However, biotite does not appear to be an alteration product of hornblende in any Walker Creek intrusion samples investigated, suggesting that biotite is at least partly igneous in origin, and not solely the result of metamorphism. Biotite is commonly dispersed throughout the groundmass, but in some samples is a micro-phenocryst (~1.5 times the size of the groundmass crystals).

Muscovite (10% to 20% of rock volume) occurs in most of the Walker Creek intrusions. It is primarily a groundmass phase, but also occurs as larger grains, as well as in pressure shadows (discussed above). Groundmass muscovite is commonly preferentially oriented, but coarser-grained muscovite is commonly bent and fractured, with fracture planes slightly discordant to the fabric defined by groundmass muscovite.

Other minerals in the Walker Creek intrusion samples include garnet (<5%), apatite (trace amounts), titanite (trace amounts), and opaques. Garnet occurs as large groundmass crystals (<1 mm) and small phenocryst grains (<2 mm) in several Walker Creek samples. Most of the garnets do not contain inclusions, nor do they have pressure shadows developed around them. This relation suggests that most of the garnet in the Walker Creek intrusions is primary (igneous). Apatite occurs as small (<0.1 mm) nonaligned inclusions in plagioclase crystals. Opaque minerals in the Walker Creek intrusions include magnetite, hematite, and minor chalcopyrite.

Major and trace element analyses and CIPW norms for seven samples (Table 1) support a sedimentary source for the Walker Creek intrusions. All but one are peraluminous, and all but two are sodic. Trace element profiles (Fig. 3C) of the most primitive intrusions (those with highest Mg/Fe, Ca/Na, V, Cr, and Ni) are similar to those of the Jordan River metagranodiorite and the Leech River Schist. The more evolved samples generally have lower trace element abundances.

Petrogenetic modeling carried out by Groome (2000) suggests that the Walker Creek intrusions were derived through (1) partial melting of the Leech River Schist, (2) magma mixing with the Tripp Creek metabasite (or other N-MORB magma), and (3) fractional crystallization. The peraluminous nature of the Walker Creek intrusions, and the abundance of metapelitic xenoliths, point toward the Leech River Schist as a potential source rock (at greater crustal depths). However, melting models using multiple trace elements indicated that the Leech River Schist is an unlikely source for the evolved compositions of the Walker Creek intrusions, and could be the source of the most primitive Walker Creek intrusions only if the schist underwent partial melting in excess of about 70% (high degrees of partial melting would also yield a match with the Jordan River metagranodiorite). At a lower and more reasonable degree of anatexis, e.g., 10%, the resultant liquid has a trace element profile dissimilar to the Walker Creek intrusions. However, mixing of this anatectic liquid with a magma equivalent to the Tripp Creek metabasite yields a composition similar to that of the most primitive Walker Creek intrusions (and the Jordan River metagranodiorite). The Tripp Creek metabasite was chosen as a mixing component in the model because field relations indicate that this unit may have been present as a magma at the time of generation of the Walker Creek intrusions. A generic N-MORB composition provides similar results. Modeling of fractional crystallization from this hybrid magma yielded compositions similar to those of the more evolved Walker Creek intrusions.

GEOCHRONOLOGY OF THE LEECH RIVER COMPLEX

Conventional U-Pb dating of zircon, titanite, and monazite, and $^{40}Ar/^{39}Ar$ dating of muscovite and biotite, provide new constraints on the depositional, magmatic/metamorphic and cooling histories of the Leech River Complex. Prior to these new isotopic ages, the only direct age constraints on the Leech River Complex were a 39 Ma K-Ar cooling date on muscovite of the Walker Creek intrusions (Fairchild and Cowan, 1982), and Rb-Sr data that Fairchild and Cowan (1982) interpreted to indicate a Jura-Cretaceous depositional age.

U-Pb Dating

Detrital Zircons from the Leech River Schist

Metasedimentary staurolite-grade Leech River Schist (sample WG99-ST) was sampled for U-Pb dating of metamorphic titanite or monazite and detrital zircon, if present. Titanite and detrital zircon were recovered, but the sample did not yield monazite. Titanite analyses were attempted, but the material was not suitable for U-Pb dating, due to very low U concentrations (~0.5–1.5 ppm) and high common Pb (>90% of total Pb was nonradiogenic). The sample did yield a small quantity (12 grains) of sufficiently coarse (>100 µm) clear, colorless detrital zircon for single-grain analysis. After strong abrasion, 8 of these grains were selected for analysis. Results are listed in Table 2 and plotted on Figure 8.

Grains A and C are 6% and 13% discordant, and yielded $^{207}Pb/^{206}Pb$ dates of ca. 1389 Ma and 1376 Ma, respectively (Table 2). Due to their significant discordance, these dates are not considered to be reliable age indicators. However, reliably dated detrital zircons that gave similar ages are known in miogeoclinal and pericratonic sedimentary and metasedimentary rocks from southern British Columbia and the western Cordillera of the conterminous United States; grains of this age are not common in the northern Canadian Cordillera (Ross and Parrish, 1991; Gehrels et al., 1995).

The remaining six detrital zircon grains gave Mesozoic Pb/U results. Four are concordant and two are strongly discordant;

TABLE 2. GEOCHRONOLOGY ANALYTICAL DATA FOR ROCKS OF THE LEECH RIVER COMPLEX

U-PB Analytical Data

Fraction[†]	Wt	U[§]	Pb*[#]	^{206}Pb[††]	Pb[§§]	^{208}Pb[##]	Isotopic ratios (1σ,%)[†††]			Apparent ages (2σ,Ma)[†††]		
	(mg)	(ppm)	(ppm)	^{204}Pb	(pg)	(%)	$^{206}Pb/^{238}U$	$^{207}Pb/^{235}U$	$^{207}Pb/^{206}Pb$	$^{206}Pb/^{238}U$	$^{207}Pb/^{235}U$	$^{207}Pb/^{206}Pb$
WG98-1-1-1C												
M2 m,e,p,12	0.041	1656	75	629	55	84	0.00795 (0.12)	0.0513 (0.37)	0.04675 (0.29)	51.1 (0.1)	50.8 (0.4)	36 (13)
M3 f,t,13	0.042	1662	59	725	48	80	0.00770 (0.22)	0.0503 (0.53)	0.04734 (0.44)	49.4 (0.2)	49.8 (0.5)	67 (21)
M4 ff,e,p,9	0.018	1129	41	664	16	80	0.00798 (0.13)	0.0515 (0.49)	0.04676 (0.43)	51.3 (0.1)	51.0 (0.5)	37 (21)
C c,cl,s,p,1	0.020	347	24	8192	3.6	7.2	0.06777 (0.11)	0.7373 (0.17)	0.07891 (0.08)	422.7 (0.9)	560.8 (1.4)	1169.8 (3.1)
D m,cl,p,3	0.016	335	49	19580	2.5	6.6	0.14621 (0.11)	1.7584 (0.16)	0.08723 (0.08)	879.7 (1.7)	1030.2 (2.1)	1365.5 (2.9)
E f,cl,p,s,5	0.014	183	8.4	2606	2.7	12	0.04325 (0.13)	0.4765 (0.18)	0.07990 (0.13)	273.0 (0.7)	395.7 (1.2)	1194.5 (5.1)
F ff,cl,p,s,15	0.011	301	30	7244	2.8	7.2	0.09778 (0.11)	1.1755 (0.17)	0.08719 (0.09)	601.4 (1.3)	789.2 (1.9)	1364.7 (3.4)
G f,b,p,e,2	0.005	4727	31	3128	3.5	0.2	0.00735 (0.10)	0.0480 (0.20)	0.04736 (0.14)	47.2 (0.1)	47.6 (0.2)	67.4 (6.5)
H ff,b,p,e,20	0.016	10280	69	430	186	0.8	0.00737 (0.16)	0.0482 (0.55)	0.04739 (0.46)	47.4 (0.2)	47.8 (0.5)	69 (22)
WG98-5-4-1C												
M1 c,cl,10	0.075	2224	93	129	776	82	0.00803 (0.53)	0.0511 (1.8)	0.04619 (1.5)	51.6 (0.5)	50.6 (1.8)	8 (71/74)
M3 m,cl,12	0.063	2122	91	126	627	83	0.00790 (0.54)	0.0513 (1.8)	0.04710 (1.5)	50.7 (0.5)	50.8 (1.8)	54 (68/71)
M4 m,cl,11	0.058	2008	85	160	412	83	0.00793 (0.32)	0.0512 (1.3)	0.04679 (1.1)	50.9 (0.3)	50.7 (1.3)	39 (53/55)
A m,b,cl,e,p,5	0.010	3781	28	1696	11	3.2	0.00799 (0.16)	0.0521 (0.34)	0.04729 (0.28)	51.3 (0.2)	51.5 (0.3)	64 (13/14)
B m,b,e,16	0.027	8063	59	1959	55	3.0	0.00783 (0.13)	0.0521 (0.25)	0.04828 (0.17)	50.3 (0.1)	51.6 (0.3)	113.2 (8.2)
C m,b,e,8	0.011	9949	72	1614	34	3.1	0.00775 (0.14)	0.0505 (0.26)	0.04724 (0.17)	49.8 (0.1)	50.0 (0.3)	61.3 (8.0)
D c,p,10	0.027	302	41	5055	14	4.1	0.13774 (0.27)	2.0588 (0.30)	0.10841 (0.08)	831.9 (4.2)	1135.2 (4.0)	1772.8 (3.0)
E c,p,5	0.023	766	17	3833	6.3	11.2	0.02196 (0.14)	0.2191 (0.21)	0.07236 (0.12)	140.0 (0.4)	201.2 (0.8)	996.0 (4.9)
WG98-32-2-1												
A c,cl,p,s,3	0.068	398	9.0	3520	11	8.0	0.02290 (0.23)	0.1567 (0.29)	0.04962 (0.18)	146.0 (0.7)	147.8 (0.8)	177 (8.5)
B c,cl,p,s,8	0.086	198	2.9	171	104	10.4	0.01456 (0.38)	0.1014 (1.2)	0.05052 (0.98)	93.2 (0.7)	98.1 (2.3)	219 (45/46)
C c,cl,s,p,12	0.075	250	10	295	172	6.5	0.03974 (0.24)	0.3965 (0.52)	0.07237 (0.38)	251.2 (1.2)	339.1 (3.0)	996 (15/16)
D m,cl,p,s,4	0.052	274	14	8057	5.6	7.8	0.05048 (0.09)	0.5461 (0.16)	0.07846 (0.08)	317.5 (0.6)	442.5 (1.1)	1158.5 (3.1)
E m,cl,p,e	0.093	701	45	57738	4.6	6.2	0.06505 (0.08)	0.7621 (0.14)	0.08498 (0.07)	406.2 (0.6)	575.2 (1.3)	1315.0 (2.8)
F f,cl,p,e	0.030	405	22	14542	2.7	9.4	0.05211 (0.09)	0.5980 (0.15)	0.08324 (0.08)	327.4 (0.6)	476.0 (1.1)	1274.8 (2.9)
G c,p,s,1	0.005	904	153	11731	2.7	5.4	0.17362 (0.13)	1.7788 (0.18)	0.07431 (0.08)	1032.0 (2.5)	1037.7 (2.4)	1049.8 (3.3)
H c,p,s,1	0.004	148	46	4599	2.4	9.4	0.29367 (0.13)	4.3878 (0.18)	0.10836 (0.09)	1659.9 (3.8)	1710 (3.0)	1772.1 (3.2)
T1 c	0.185	111	2.6	44	708	47	0.01360 (2.2)	0.0877 (7.6)	0.04678 (6.4)	87.1 (3.8)	85 (13)	38 (280/338)
T2 m	0.125	254	4.0	146	218	22	0.01377 (0.46)	0.0926 (1.7)	0.04875 (1.4)	88.2 (0.8)	89.9 (2.9)	136 (65/68)

(continued)

TABLE 2. GEOCHRONOLOGY ANALYTICAL DATA FOR ROCKS OF THE LEECH RIVER COMPLEX (continued)

U-PB Analytical Data												
Fraction[†]	Wt	U[§]	Pb*[#]	^{206}Pb[††]	Pb[§§]	^{208}Pb[##]	Isotopic ratios (1σ,%)[†††]			Apparent ages (2σ,Ma)[†††]		
	(mg)	(ppm)	(ppm)	^{204}Pb	(pg)	(%)	$^{206}Pb/^{238}U$	$^{207}Pb/^{235}U$	$^{207}Pb/^{206}Pb$	$^{206}Pb/^{238}U$	$^{207}Pb/^{235}U$	$^{207}Pb/^{206}Pb$
WG98-7-1-1C												
A c,cl,p,s,5	0.070	329	8.6	5891	6.2	12	0.02532 (0.14)	0.1739 (0.19)	0.04980 (0.10)	161.2 (0.4)	162.8 (0.6)	185.8 (4.5)
B c,cl,p,s,5	0.055	698	45	28588	5.5	5.7	0.06585 (0.33)	0.7268 (0.36)	0.08005 (0.08)	411.1 (2.7)	554.7 (3.0)	1198.1 (3.3)
C c,cl,p,11	0.040	711	12	8720	3.6	7.4	0.01766 (0.11)	0.1515 (0.16)	0.06224 (0.09)	112.8 (.02)	682.4 (0.4)	682.4 (3.8)
D c,cl,p,e,6	0.052	556	39	14730	8.8	3.6	0.07212 (0.11)	0.8056 (0.17)	0.08101 (0.07)	448.9 (1.0)	600.0 (1.5)	1221.7 (2.9)
E c,p,16	0.074	219	8.0	3121	11.8	12	0.03481 (0.09)	0.3464 (0.17)	0.07218 (0.09)	220.6 (0.4)	302.0 (0.9)	990.9 (3.8)
F m,p,e,20	0.023	378	22	13891	2.3	8.0	0.05799 (0.09)	0.7744 (0.15)	0.09685 (0.07)	363.4 (0.6)	582.3 (1.3)	1564.2 (2.8)
I c,pi,p,e,1	0.009	420	96	1365	37	8.2	0.22350 (0.22)	2.7808 (0.30)	0.09024 (0.13)	1300.3 (5.2)	1350.4 (4.4)	1430.6 (4.9)
J c,pi,p,s,1	0.010	217	57	2565	13	5.9	0.26124 (0.11)	3.6746 (0.18)	0.10201 (0.10)	1496.2 (2.9)	1565.9 (2.9)	1661.1 (3.6)
WG99ST												
A m,cl,co,br,1	0.002	1329	294	27464	1.4	4.5	0.22595 (0.10)	2.7513 (0.16)	0.08831 (0.08)	1313.2 (2.5)	1342.4 (2.4)	1389.3 (2.9)
B m,cl,co,br,1	0.002	63	1.4	136	1.4	11	0.02192 (0.54)	0.2016 (2.1)	0.06671 (2.0)	139.8 (1.5)	186.5 (7.2)	828 (82/86)
C m,cl,co,br,1	0.003	389	80	2450	6.0	5.8	0.20703 (0.12)	2.5033 (0.19)	0.08769 (0.11)	1213.0 (2.8)	1273.0 (2.8)	1375.8 (4.2)
D m,cl,co,e,1	0.002	723	20	469	5.3	11	0.02700 (0.15)	0.1843 (0.57)	0.04951 (0.51)	171.7 (0.5)	171.8 (1.8)	172.2 (23/24)
E m,cl,co,e,1	0.002	136	3.0	87	5.6	7.5	0.02274 (0.44)	0.1546 (3.5)	0.04930 (3.3)	144.9 (1.3)	145.9 (9.6)	162 (147/162)
F m,cl,co,e,1	0.004	1021	29	851	8.9	6.5	0.02916 (0.14)	0.2005 (0.42)	0.04986 (0.35)	185.3 (0.5)	185.5 (1.4)	189 (16/17)
G m,cl,co,e,1	0.002	1280	21	474	5.6	10	0.01612 (0.16)	0.1069 (0.88)	0.04813 (0.83)	103.1 (0.3)	103.2 (1.7)	106 (39/40)
H m,cl,co,st,1	0.002	544	16	368	5.0	17	0.02573 (0.32)	0.2653 (0.75)	0.07478 (0.68)	163.8 (1.0)	238.9 (3.2)	1063 (27/28)

[†] Upper case letter—zircon fraction identifier. All zircon fractions air abraded except WG98-1-1-1C: G and H. Monazites and titanites not abraded. Grain size, intermediate dimension: c—>134mm, m—<134mm and >104mm, f—<104mm and >74mm, ff <74mm. Grain character codes: b—brown, br—broken pieces, cl—clear, co—colorless, e—elongate, p—prismatic, pi—pink, s—stubby, t—tabular. The last numeral represents number of grains analyzed if 20 or less. Zircons nonmagnetic on Franz magnetic separator at field strength of 1.8A and sideslopes of 1°–5°. Monazites and titanites nonmagnetic at 0.6A and magnetic at 1.8A and 20° sideslope. Front slope of 20° for all.

[§] U blank correction of 1pg ± 20%; U fractionation corrections were measured for each run with a double 233U-235U spike (about 0.004/amu).

[#] Radiogenic Pb.

[††] Measured ratio corrected for spike and Pb fractionation of 0.0035/amu ± 20% (Daly collector) which was determined by repeated analysis of NBS Pb 981 standard throughout the course of this study.

[§§] Total common Pb in analysis based on blank isotopic composition.

[##] Radiogenic Pb.

[†††] Corrected for blank Pb (1-4 pg, throughout the course of this study), U (1 pg) and common Pb concentrations based on Stacey Kramer's model Pb at the age of the rock or the 207Pb/206Pb age of the rock.

(continued)

TABLE 2. GEOCHRONOLOGY ANALYTICAL DATA FOR ROCKS OF THE LEECH RIVER COMPLEX (continued)

$^{40}Ar/^{39}Ar$ Analytical Data
WG98 1-1-1C White Mica

Weighted average of J from standards = 0.008484 ± 0.000029

Laser Power (mW)	Cumulative ^{39}Ar	$^{40}Ar/^{39}Ar$ measured	37Ar/39Ar measured	$^{36}Ar/^{39}Ar$ measured	Atmospheric ^{40}Ar (%)	Ca/K	±	Cl/K	±	40*/39K	±	Age (Ma)	± (Ma)
150	0.0013	29.97307	0.03471	0.09346	92.21999	0.06368	0.01904	0.0042	0.00103	2.32973	1.10025	35.31	16.51
300	0.0044	9.2029	0.028	0.02348	75.59119	0.05138	0.0118	0.00102	0.00062	2.23935	0.70233	33.95	10.55
450	0.0126	6.31856	0.016	0.01151	54.07474	0.02936	0.00683	0.00061	0.00014	2.88867	0.22819	43.68	3.41
600	0.0276	7.78988	0.00758	0.0153	58.23978	0.0139	0.00204	0.00052	0.00023	3.2411	0.07793	48.94	1.16
800	0.0628	6.12156	0.00243	0.01079	52.34594	0.00446	0.0009	0.0003	0.00008	2.9035	0.06375	43.9	0.95
1000	0.1446	3.79326	0.00025	0.00258	20.28835	0.00045	0.00058	0.00042	0.00003	3.00079	0.02805	45.35	0.42
1250	0.2611	3.85587	0.00013	0.00282	21.78205	0.00024	0.00024	0.00038	0.00004	2.99353	0.02656	45.25	0.4
1500	0.4083	3.87075	0.00028	0.00291	22.36911	0.00051	0.00031	0.00039	0.00004	2.98262	0.02037	45.08	0.3
2000	0.64	3.6225	0.0003	0.00193	15.89645	0.00056	0.00016	0.0004	0.00003	3.02252	0.01118	45.68	0.17
2500	0.8212	3.38153	0.00013	0.00132	11.67189	0.00024	0.00019	0.00043	0.00002	2.96149	0.011	44.77	0.16
3500	0.9018	3.10283	-0.0002	0.00036	3.48614	-0.00037	0.0005	0.00038	0.00007	2.96696	0.02018	44.85	0.3
4000	0.9153	3.10143	0.00058	0.00111	10.65845	0.00106	0.00167	0.00067	0.00027	2.74522	0.12819	41.54	1.92
8500	1	3.06857	-0.00051	0.00014	1.32106	-0.00094	0.00034	0.00037	0.00003	2.99971	0.01498	45.34	0.22
Integrated		3.78538	0.00058	0.00261	20.54261	0.00106	0.00013	0.00041	0.00001	2.98496	0.00764	45.12	0.19
Plateau	45.2 ± 0.2												
Isochron	45.0 ± 0.3		40/36i =	301.8 ± 6.0									

$^{40}Ar/^{39}Ar$ Analytical Data
WG98-4-6-1C Biotite

Weighted average of J from standards = 0.008484 ± 0.000029

Laser Power (mW)	Cumulative ^{39}Ar	$^{40}Ar/^{39}Ar$ measured	$^{37}Ar/^{39}Ar$ measured	$^{36}Ar/^{39}Ar$ measured	Atmospheric ^{40}Ar (%)	Ca/K	±	Cl/K	±	40*/39K	±	Age (Ma)	± (Ma)
150	0.0074	75.87774	0.02135	0.25531	99.46564	0.03918	0.00539	0.00084	0.00019	0.40532	0.62096	6.19	9.47
300	0.0221	16.47513	0.01108	0.04742	85.20272	0.02033	0.0024	0.0009	0.00013	2.43364	0.17192	36.87	2.58
450	0.069	6.01006	0.00783	0.01135	56.08662	0.01436	0.0007	0.00064	0.00011	2.62663	0.10589	39.76	1.59
600	0.1378	4.80107	0.01099	0.00674	41.7284	0.02016	0.0007	0.00056	0.00007	2.78096	0.0588	42.07	0.88
800	0.2072	4.28869	0.01475	0.00502	34.80232	0.02706	0.00068	0.00052	0.00007	2.77744	0.05226	42.02	0.78
1000	0.2985	3.82709	0.02157	0.00336	26.13574	0.03957	0.0006	0.00056	0.00004	2.80569	0.03841	42.44	0.57
1250	0.4123	4.06778	0.02425	0.00418	30.54542	0.0445	0.00078	0.00049	0.00003	2.80537	0.03497	42.43	0.52
1500	0.525	3.85028	0.022	0.00345	26.62076	0.04037	0.0007	0.00049	0.00005	2.80428	0.03406	42.42	0.51
2000	0.6913	3.60386	0.03814	0.00261	21.47938	0.06998	0.00056	0.0005	0.00003	2.80731	0.01728	42.46	0.26
2500	0.8217	3.62523	0.04806	0.00263	21.4696	0.08818	0.00057	0.00051	0.00004	2.82446	0.03067	42.72	0.46
3500	0.8638	3.70205	0.04145	0.00268	21.48364	0.07605	0.00152	0.00049	0.00011	2.88426	0.07968	43.61	1.19
4000	0.9612	3.74785	0.04861	0.00307	24.27361	0.08919	0.00143	0.00058	0.00006	2.81647	0.02781	42.6	0.42
8500	1	3.21913	0.02964	0.00094	8.61091	0.0544	0.0012	0.00057	0.0001	2.91576	0.0632	44.08	0.94
Integrated		4.67665	0.02991	0.00632	40.15576	0.05489	0.00026	0.00053	0.00002	2.78158	0.01316	42.08	0.24
Plateau	42.5 ± 0.2												
Isochron	43.0 ± 0.2		40/36i =	285.8 ± 2.0									

the latter two are likely to contain old inherited cores. The four concordant grains gave $^{206}Pb/^{238}U$ dates of ca. 185, 172, 145 and 103 Ma, which are interpreted as good estimates of their magmatic ages. The youngest grain, which gave concordant results at 103 Ma (grain G), was an elongate prism interpreted as a detrital zircon of igneous origin. The interpreted age of this grain indicates that the sedimentary protolith of this schist, and probably much of the metasedimentary component of the Leech River Complex, was deposited after ca. 103 Ma. The two older concordant grains give ages typical for the Island Intrusions and Westcoast Crystalline Complex of Wrangellia on Vancouver Island (DeBari et al., 1999), and the younger two concordant grains have interpreted ages common in the southern Coast Plutonic Complex (Friedman and Armstrong, 1995). However, igneous rocks of these ages are known along the length of the Cordillera and are thus not latitudinally significant. Discordant grains B and H appear to contain significant old inheritance and were probably derived from igneous rocks that intruded crust containing components of old zircon. Candidates for such crust include North American continental crust, overlying miogeoclinal sequences, and flanking pericratonic terranes.

Igneous Rocks of the Leech River Complex

The Jordan River metagranodiorite was sampled for U-Pb dating at two localities (Fig. 2). Both samples (WG98-32-2-1C and WG98-7-3-2C) are fine-grained, foliated granodiorites. Zircon recovered from these consists of clear, colorless, euhedral grains and rare, clear, pink grains. In addition, a small

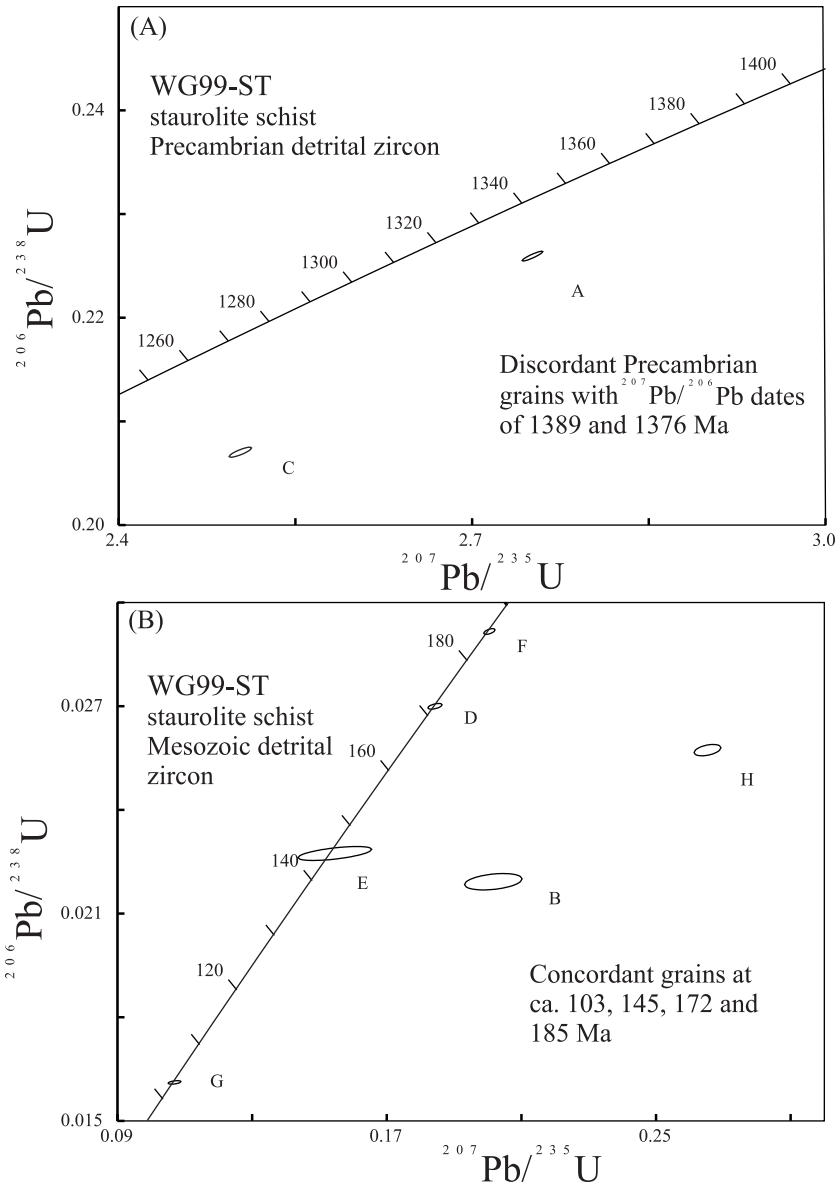

Figure 8. Concordia plots showing U-Pb results for sample WG99-ST. U-Pb analytical data are presented in Table 2 and plotted at the 2 level of uncertainty. A: Detail of Precambrian grains. B: Detail of Mesozoic grains. All fractions are single grain analyses. A and C are stubby, pink zircon grains; all other fractions are colorless stubby fractions.

quantity of clear, yellow titanite was recovered from one of the samples (WG98-32-2-1C).

Discordant results for multi-grain, colorless zircon fractions from both samples indicate the presence of Precambrian to Mesozoic inheritence but do not lead to a precise age estimate for the intrusion (Figs. 9, 10). Single pink grains analyzed from both samples also give discordant results, with $^{207}Pb/^{206}Pb$ dates ranging from 1050 to 1800 Ma. Based on their distinctive physical characteristics and U-Pb systematics, pink zircons are interpreted as Precambrian xenocrysts. Concordant overlapping results were obtained for two multi-grain titanite fractions. Relatively precise fraction T2, with a $^{206}Pb/^{238}U$ date of 88.2 ± 0.8 Ma is interpreted as the time at which the Jordan River metagranodiorite (sample WG98-32-2-1; Fig. 10B) cooled below the closure temperature for titanite, which is estimated to be 660 °C or greater (Frost et al., 2000). Thus, this titanite date is interpreted as the crystallization age for the Jordan River metagranodiorite. Results for discordant zircon fraction B (Fig. 10B) nearly overlap with those of the titanites (Table 2), which supports the interpreted Late Cretaceous age.

The Walker Creek tonalite-trondhjemite-granodiorite suite of intrusions was sampled for U-Pb dating at two localities: one

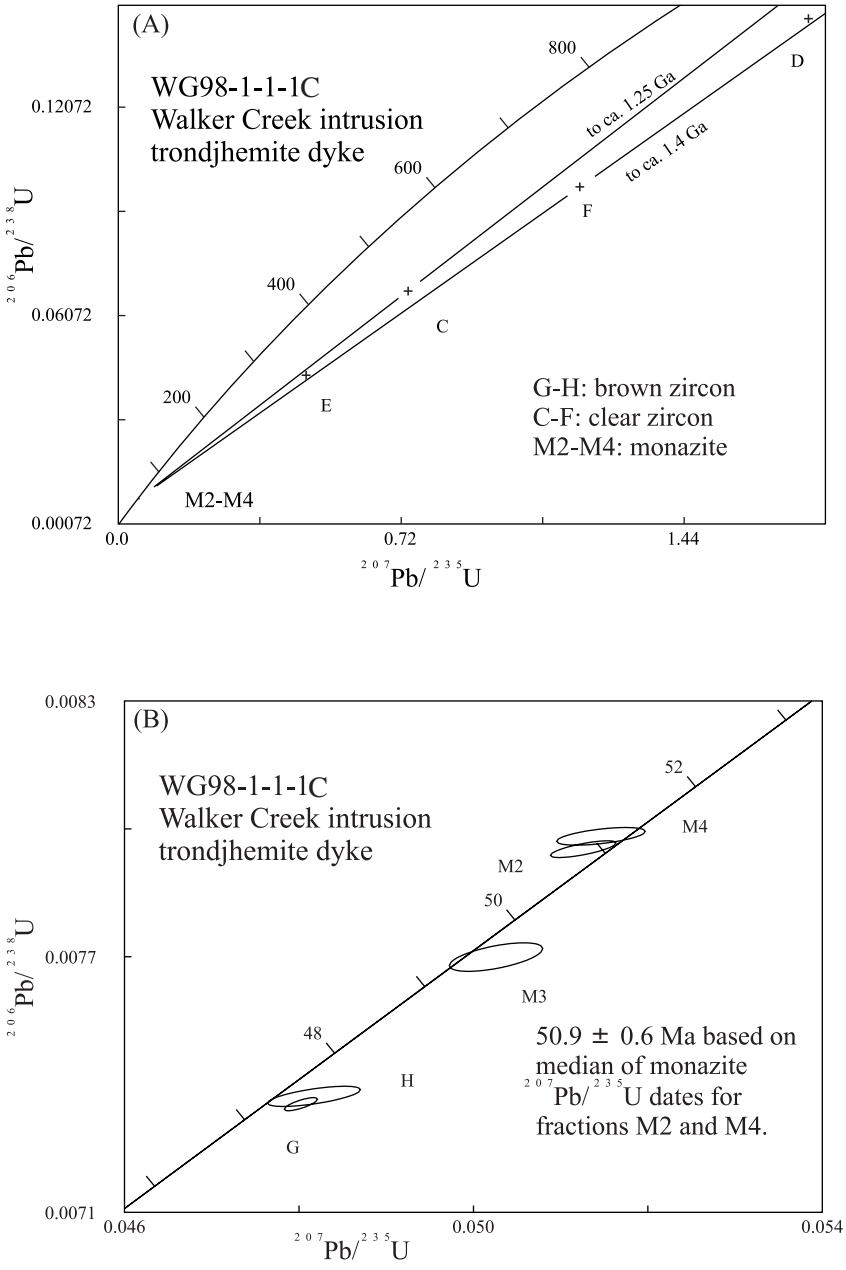

Figure 9. Concordia plots showing U-Pb results for sample WG98-1-1-1C (Walker Creek intrusion). U-Pb analytical data are presented in Table 2 and plotted at the 2 level of uncertainty. A: All fractions. B: Expanded plot showing detail of monazite and brown zircon fractions.

from within a swarm (foliated trondhjemite, WG98-1-1-1C), and the other from an isolated intrusion (weakly foliated tonalite, WG98-5-4-1C; Fig. 2). Monazite and two populations of zircon were recovered and analyzed from each sample. One zircon population consisted of clear, colorless, equant to stubby grains, and the other was made up of brown, elongate prisms. Cores and zoning were not observed in either zircon type. Monazites were clear, pale yellow, nearly inclusion-free, subhedral grains.

Multi-grain clear zircon fractions from both samples yielded discordant results, with $^{207}Pb/^{206}Pb$ dates ranging from 1000 Ma to 1800 Ma, indicating the presence of significant components of old inherited zircon, which appears to occur as cryptic cores (Figs. 11A, 11B; Table 2). Multi-grain brown zircon fractions from both samples contain high concentrations of uranium (~4000–10,000 ppm; Table 2), and give slightly discordant results, with Pb/U dates of 47 Ma to 51 Ma. The slight discordance is attributed to minor inherited zircon, and for most fractions, minor Pb loss (Figs. 11B, 12B). Multi-grain monazite fractions from both samples are concordant to reversely discordant. Interpreted igneous crystallization ages are based on median $^{207}Pb/^{235}U$ dates: 50.9 ± 0.6 Ma for sample WG98-1-1-1C (fractions M2 and M4) and 50.7 ± 1.9 Ma for sample WG98-5-4-1C (fractions M1, M3, and M4) (Figs. 9 and 10 respectively). Discordia lines fit from the interpreted igneous age of each rock, through discordant clear zircon fractions, give upper intercept ages of 1250 Ma to 1800 Ma, which are interpreted as the range of average ages of inherited zircon in the clear grains (Figs. 12A, 12B).

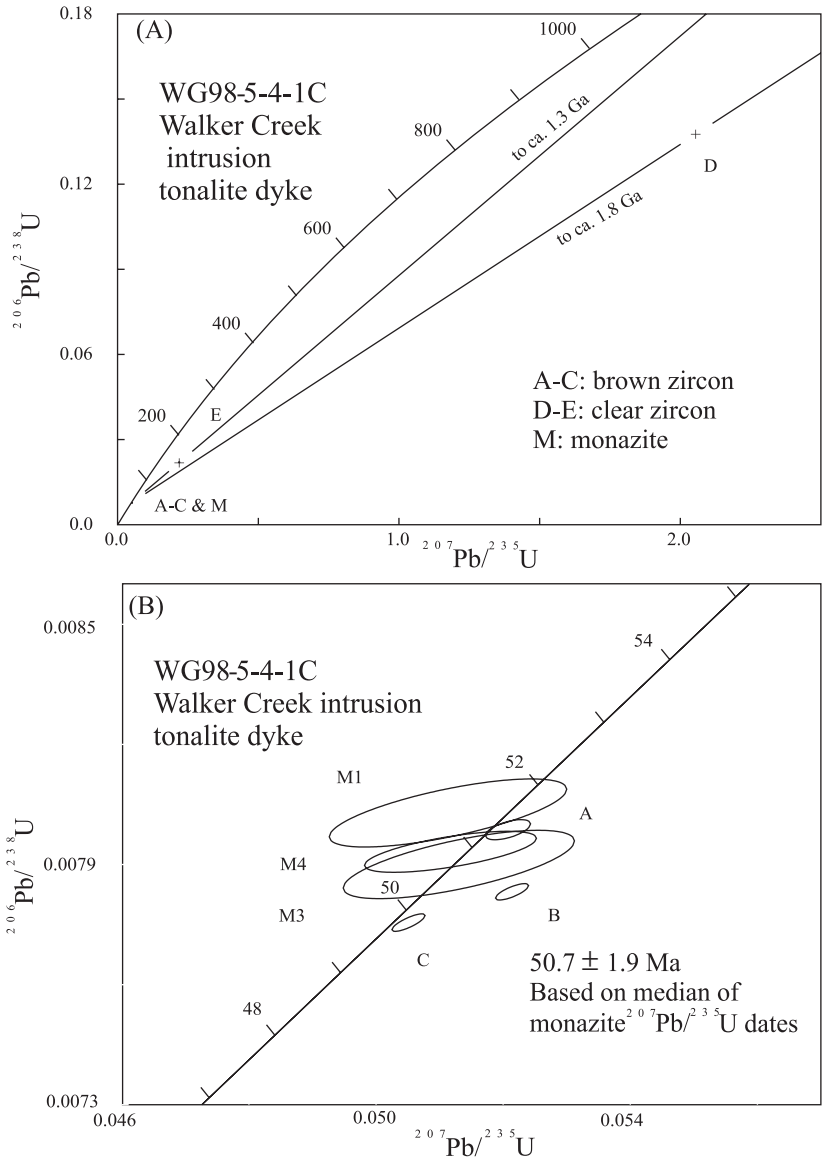

Figure 10. Concordia plots showing U-Pb results for sample WG98-5-4-1C (Walker Creek intrusion). U-Pb analytical data are presented in Table 2 and plotted at the 2 level of uncertainty. A: All fractions. B: Expanded plot showing detail of monazite and brown zircon fractions.

$^{40}Ar/^{39}Ar$ *Cooling Ages*

$^{40}Ar/^{39}Ar$ dating of two mica samples was undertaken in order to delineate a cooling history for the Leech River Complex. Muscovite was sampled from a Walker Creek intrusion (WG98-1-1-1C) (Fig. 13A), and biotite from a sample of amphibolite-facies Leech River Schist (WG98-4-6-1C) (Fig. 13B); the two sample localities are approximately 50 m apart. Plateau ages of 45.2 ± 0.2 Ma and 42.5 ± 0.2 Ma were obtained from the muscovite and biotite samples, respectively. On the basis of Ar-blocking temperatures for micas (Kirschner et al., 1996), the muscovite cooled below approximately 400 °C at ca. 45.2 Ma and the biotite cooled below approximately 330 °C at ca. 42.5 Ma.

METAMORPHISM AND DEFORMATION

Metamorphic grade within the Leech River Complex varies from chlorite zone (greenschist facies) in the north to staurolite-andalusite zone (amphibolite facies) in the south (Fairchild and Cowan, 1982; Rusmore and Cowan, 1985), a gradient that generally correlates with the increasing abundance of intrusive rocks in the southern part of the eastern Leech River Complex (Groome et al., 1999; Groome, 2000). In and near the study area, in the eastern part of the Complex, field and petrographic data indicate that there were at least two periods of metamorphism: a regional greenschist facies event and a localized amphibolite facies event spatially associated with contact aureoles adjacent to

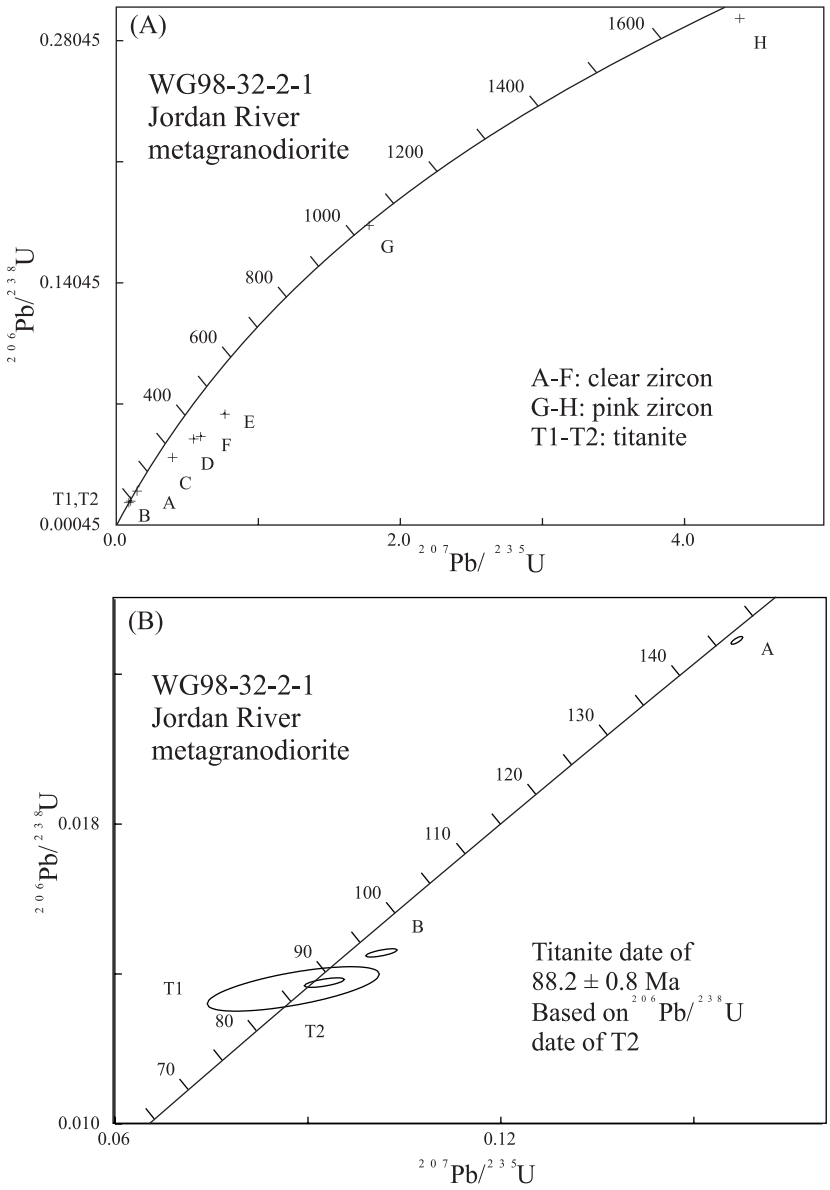

Figure 11. Concordia plots showing U-Pb results for sample WG98-32-2-1 (Jordan River metagranodiorite). U-Pb analytical data are presented in Table 2 and plotted at the 2 level of uncertainty. A: All fractions. B: Expanded plot showing detail of titanite and young zircon fractions.

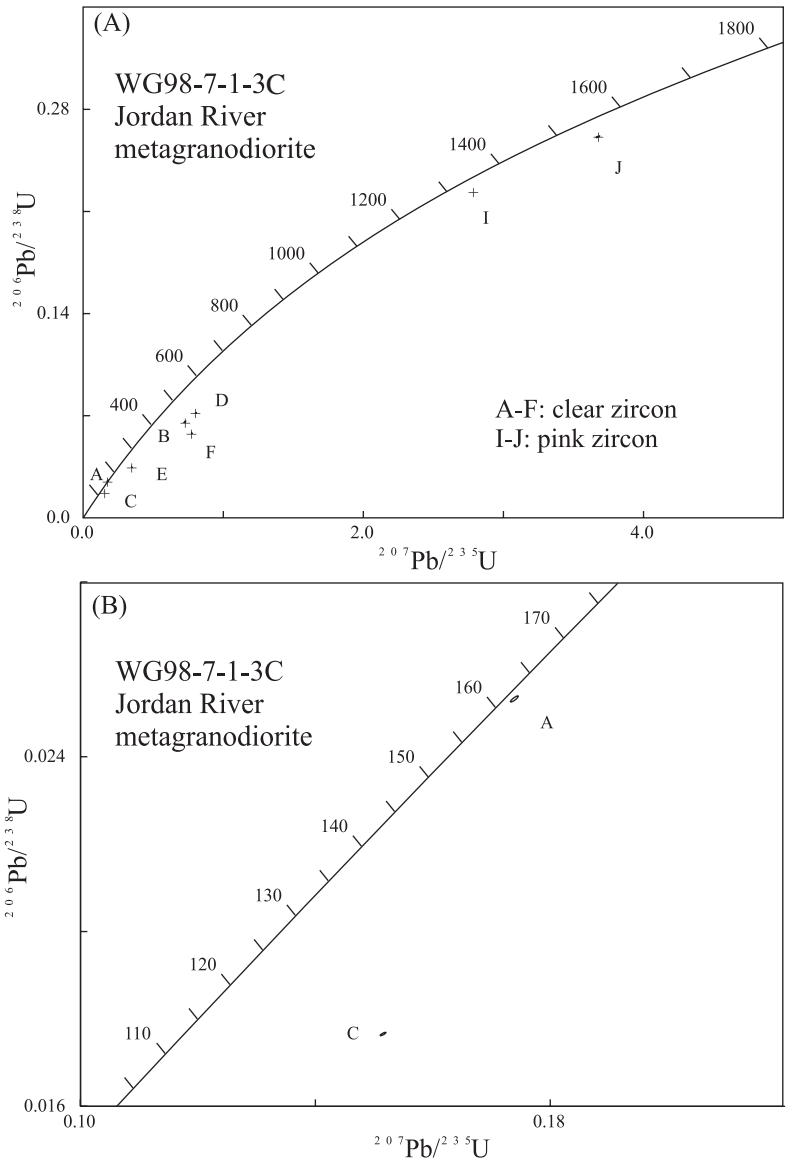

Figure 12. Concordia plots showing U-Pb results for sample WG98-7-1-3C (Jordan River metagranodiorite). U-Pb analytical data are presented in Table 2 and plotted at the 2 level of uncertainty. A: All fractions. B: Expanded plot showing detail of young zircon fractions.

intrusions (Groome, 2000). The greenschist-facies metamorphic assemblage consists primarily of biotite-chlorite-plagioclase-white mica-quartz, but biotite is locally absent in the northern parts of the Complex. The biotite-chlorite-plagioclase-white mica-quartz assemblage corresponds to a temperature range of 400–450 °C, at a pressure of approximately 3 kbar, decreasing to a temperature range of 300 to 400 °C in the absence of biotite, assuming orogenic metamorphism along the kyanite geotherm (Fig. 14) (Bucher and Frey, 1994).

The amphibolite-facies metamorphic assemblage in the Leech River Complex consists of biotite-staurolite-andalusite-plagiolcase-muscovite-quartz, ± garnet, ± cordierite. This assemblage corresponds to a temperature of 500 to 600 °C and a pressure less than the andalusite-kyanite transition, which is approximately 3.5 kbar at 620 °C (Bucher and Frey, 1994). Thus, the transition from greenschist-facies to amphibolite-facies in the study area was apparently the result of an isobaric temperature increase. This, along with the close spatial association with intrusive activity, indicates a contact metamorphic regime. A striking increase in porphyroblast size and abundance occurs at the margins of the Jordan River and Walker Creek intrusions. Staurolite is ubiquitous in the amphibolite facies schists and was used as the main indicator for the amphibolite facies. The presence of garnet and andalusite appears to be strongly controlled by protolith chemistry within the amphibolite facies, as their first occurrences are sporadic near the amphibolite-facies boundary.

Staurolite porphyroblasts range in size from 0.5 mm to 5 mm. They are usually well shaped crystals that commonly have cross-penetration twins. At several localities, staurolite porphyroblasts

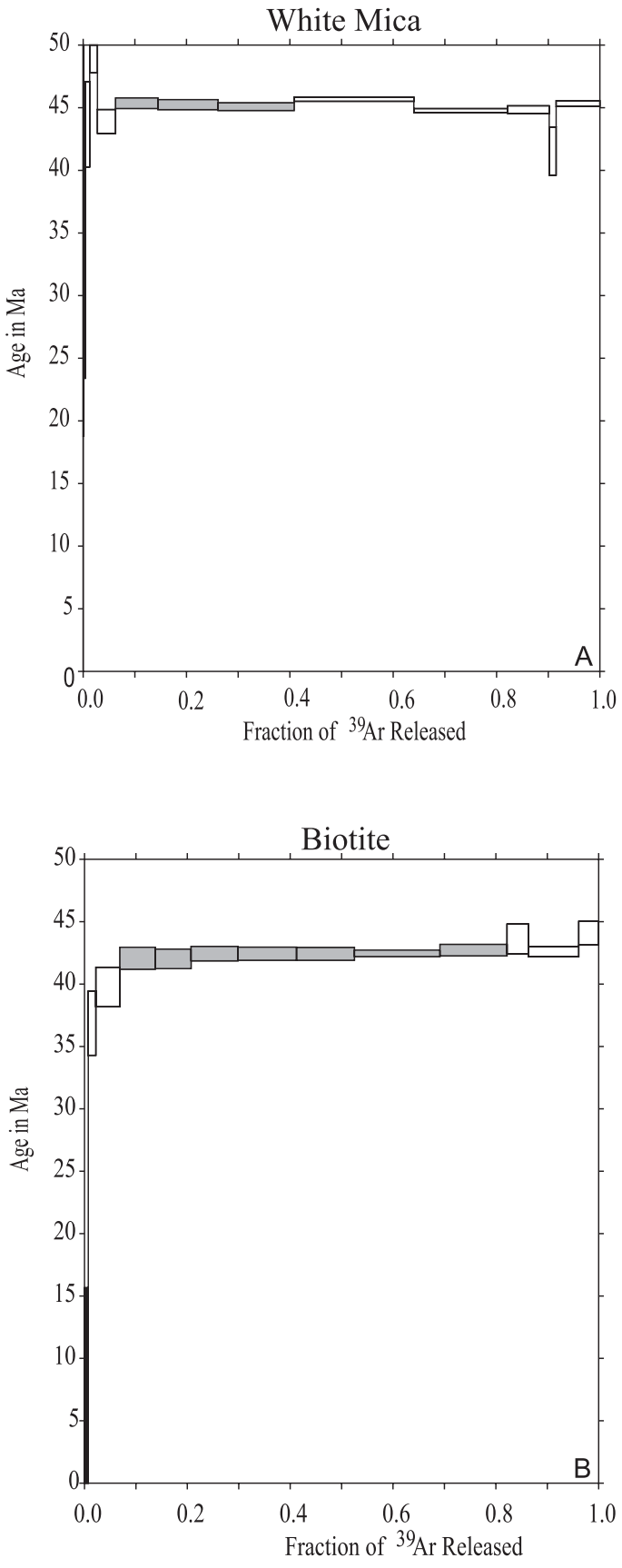

Figure 13. A: $^{40}Ar/^{39}Ar$ spectrum for white mica. Plateau age is 45.2 ± 0.2 Ma. Data are presented in Table 2. The shaded region indicates the plateaus used for the plateau age. B: $^{40}Ar/^{39}Ar$ spectrum for biotite. Plateau age is 42.5 ± 0.2 Ma. Data are presented in Table 2. The shaded region indicates the plateaus used for the plateau age.

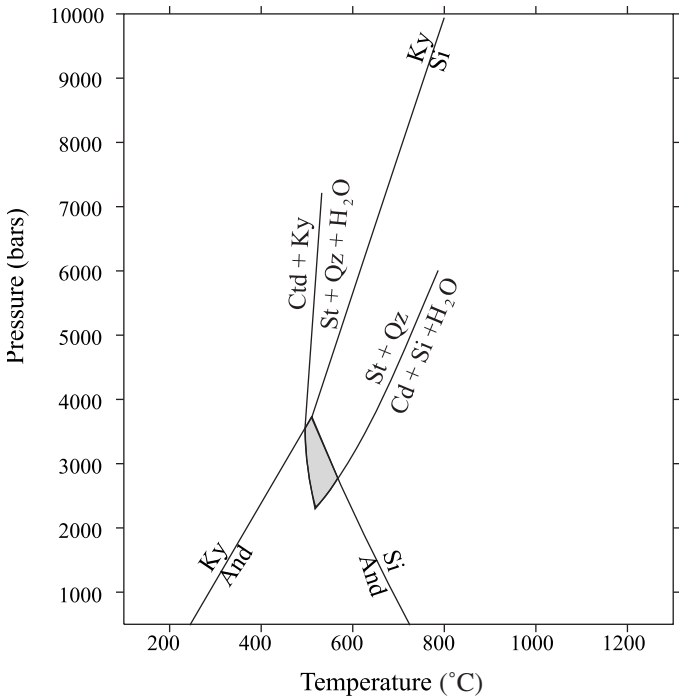

Figure 14. Pressure-temperature conditions of peak metamorphism in the Leech River Schist. Shaded region indicates the *P-T* conditions of peak metamorphism based on geothermometry and field relationships. And—andalusite, Cd—cordierite, Ctd—chloritoid, Ky—kyanite, Qz—quartz, Si—sillimanite, St—staurolite. Reactions are from Bucher and Frey (1994).

have small pressure shadows around them, indicating syn-kinematic growth (probably syn-D1). In thin section, these pressure shadows contain the same mineral assemblage as the ground mass, indicating that these porphyroblasts are not pre-kinematic, as the pressure shadows equilibrated under the same conditions as the rest of the rock (Paterson and Fowler, 1993). At other outcrops, staurolite porphyroblasts are randomly oriented and lack pressure shadows. These relations indicate that at these outcrops staurolite growth was post-kinematic and constrains the amphibolite-facies metamorphism to be syn- to post-kinematic.

The orientations of andalusite porphyroblasts also indicate that amphibolite-facies metamorphism was syn- to post-kinematic (D1). Andalusite porphyroblasts are best observed along the banks of the Jordan River. Where present, these porphyroblasts range in size from 1 cm to more than 15 cm in maximum

dimension. The length to width ratios of these porphyroblasts vary from about 1 to 10, with the smaller porphyroblasts being more equant. The highly elongate porphyroblasts are oriented parallel to the schistosity defined by biotite. Locally, some of these porphyroblasts were boudinaged, indicating that deformation had affected them. However, the more equant porphyroblasts crosscut schistosity without the development of pressure shadows. These features indicate that the latter porphyroblasts grew after development of the schistosity. Some andalusite porphyroblasts are pseudomorphed by fine-grained muscovite and biotite, indicating minor retrograde metamorphism. Garnet porphyroblasts range from 0.5 mm to 2 mm in diameter. They are most commonly associated with pressure shadows, indicating mainly syn-kinematic (D1) growth.

The contact nature of the amphibolite-facies metamorphism is supported by mineralogical variations at the margins of dikes and stocks. For example, a small contact aureole was observed in pelitic schist adjacent to a small Walker Creek dike. The visible extent of the contact zone extended less than 35 cm from the dike margin. Within 10 cm of the contact, mm-scale staurolite and garnet are present. The staurolite progressively decreases in abundance away from the dike, and is completely absent in hand specimen beyond 10 cm from the dike. The disappearance of staurolite indicates a drop in grade to the garnet zone, which extends for approximately 25 cm farther from the dike. Beyond 35 cm from the contact, garnet is not visible and the metamorphic grade in the host rock equals the regional middle-greenschist grade in the area. Alongside larger dikes, dike swarms, and stocks, similar increases in metamorphic grade are clearly evident, with broad contact aureoles extending for up to 100 m from intrusive contacts.

Fabric development and deformation of the Leech River Schist were studied by Fairchild (1979), Rusmore (1982) and Groome (2000), but remains imperfectly understood. Fairchild (1979) documented two periods of (post-depositional) deformation in the eastern Leech River Complex. He recognized an early deformational event that produced a regional cleavage in the lower-grade rocks, a foliation in the higher-grade rocks, and transposition of bedding into parallelism with the regional fabric. He also suggested that small, tight to isoclinal folds, including those defined by quartz veins, formed during this deformational this event. Fairchild (1979) recognized a second deformation that produced a localized crenulation cleavage in the lower-grade rocks and large open folds (tens of meters wavelength) in the earlier-formed foliation. These folds are larger near the Leech River fault zone and plunge shallowly to the east. Similar deformational events were reported by Rusmore (1982) in the western portion of the Leech River Complex near Port Renfrew.

Groome (2000) recognized the first and second deformation events described by Fairchild (1979), but also identified a conundrum in the timing of fabric development, igneous intrusion, and formation of contact metamorphic aureoles. Both the Walker Creek and Jordan River intrusions are parallel to the enclosing Leech River Schist, and have contact metamorphic aureoles that apparently record syn- to post-kinematic mineral growth of staurolite and andalusite. In the proximal, coarsest parts of these aureoles, the "syn-kinematic" porphyroblasts are concordant with schistosity, and are locally boudinaged and crosscut by shear bands. The "post-kinematic" porphyroblasts crosscut the schistosity, and apparently postdate the formation of foliation (Fig. 15). However, the ages of the Walker Creek and Jordan River intrusions, and by inference their aureoles, differ by nearly 40 m.y., a relation that requires two separate intervals of foliation development and "post-kinematic" mineral growth. If this is correct, the earlier interval of deformation produced a schistosity that is remarkably similar, both texturally and mineralogically, to the fabric generated by the later one. Additional structural and geochronologic studies are needed to resolve this problem, for instance, direct dating of foliation-defining minerals.

EVOLUTION OF THE LEECH RIVER COMPLEX

The Leech River Complex provides an important link between Wrangellia and other inboard terranes of western North America, and the outboard Paleogene Crescent Terrane, one of the last assemblages to accrete to the continental margin. The main events in the evolution of the complex are indicated in Figure 16. Detrital zircon ages indicate that the Leech River Complex originated as a sedimentary deposit derived from a variety of source areas, including those of Precambrian age or provenance, while whole-rock geochemistry of the metasediments indicate an arc influence for the protolith. The age of earliest sedimentation is not known, but deposition must have occurred after 103 Ma, the interpreted crystallization age of the youngest analyzed detrital zircon grain.

Deposition of the schist protolith ended prior to ca. 88 Ma when the peraluminous Jordan River metagranodiorite was emplaced at approximately 3 kbar. The cause of burial to depths of ca. 10 km is unknown, but may be related to regional west-directed thrusting along the Coast Mountains in early Late

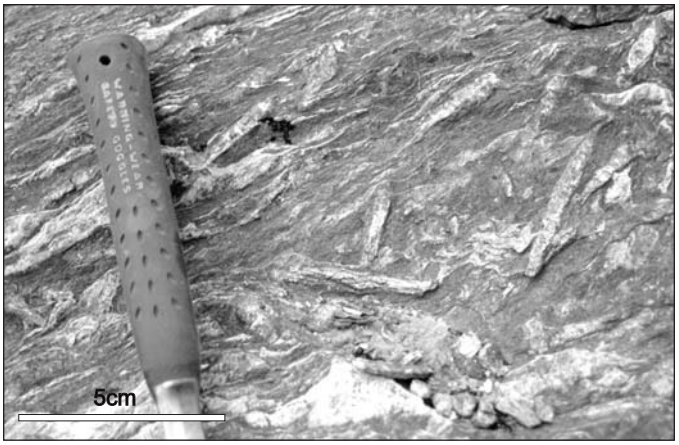

Figure 15. Photograph of randomly oriented andalusite porphyroblasts.

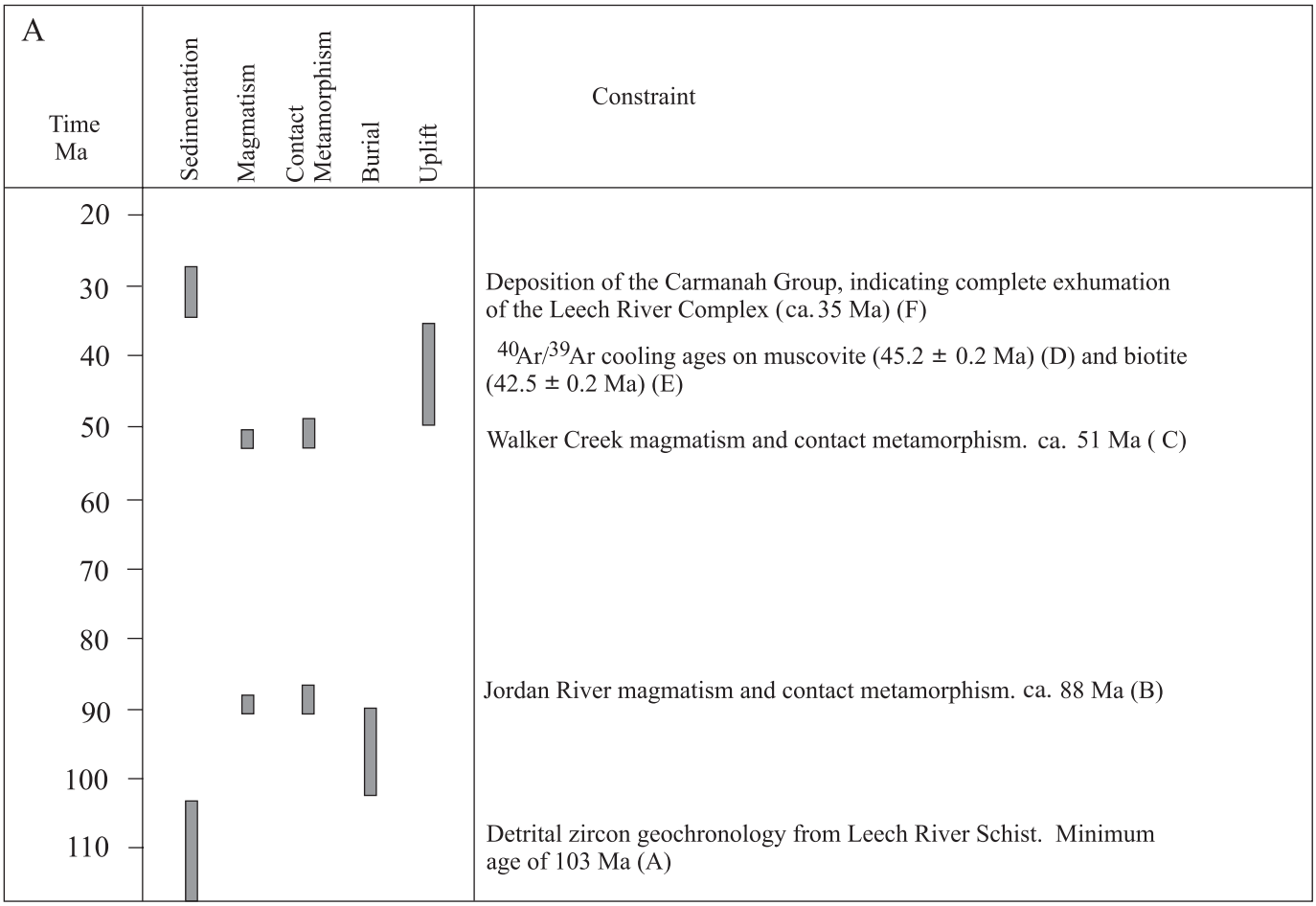

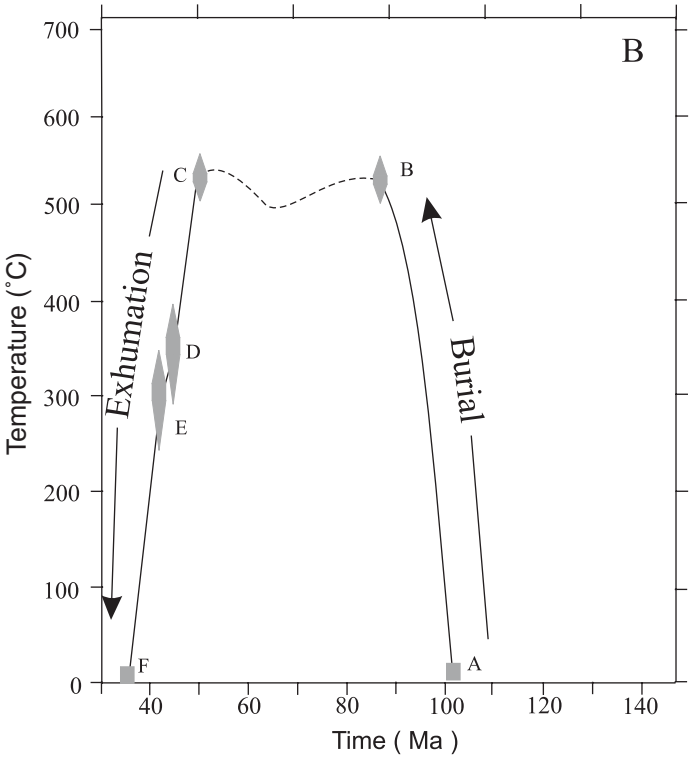

Figure 16. A: Timeline of events in the Leech River Complex based on field, geochronologic, and regional geologic constraints. B: Temperature-time path of the Leech River Complex based on field and geochronologic constraints. Letter labels correspond to the labels in A.

Cretaceous time (Brandon, 1989; Rubin et al., 1990; Journeay and Friedman, 1993). The source of the magmatism is also unknown, but the peraluminous composition of the intrusion suggests that it may have been generated, at least in part, by melting of the Leech River Schist. This forearc magmatism must have been generated by unusually high geothermal conditions, possibly during ridge subduction. The undated Tripp Creek metabasite, with its MORB character, may also have been emplaced at this time (and/or during Walker Creek magmatism), and may have provided much of the heat necessary for anatexis. Deformation, leading to schistosity in the host sediments and foliation in the intrusions, appears to have been broadly synchronous with the magmatism, with peak thermal conditions and porphyroblast growth outlasting the development of foliation.

The peraluminous Walker Creek intrusions were emplaced into the Leech River Schist at ca. 51 Ma, approximately 37 m.y. after crystallization of the Jordan River intrusion. Like the Jordan River intrusions, most of the Walker Creek intrusions are foliated, and imparted on the schist a contact aureole that outlasted deformation. Some of the Walker Creek intrusions are weakly foliated, and a few are non-foliated, indicating that magmatism continued after deformation ended. Geochemical modeling suggests that the Walker Creek intrusions evolved by anatexis or assimilation of the Leech River Schist, mixing with MORB-like melts (possibly magmas of the Tripp Creek metabasite), and fractional crystallization. Subduction of the Kula-Farallon ridge is a plausible cause of high heat flow, MORB-type magmatism, and forearc anatexis.

Rapid cooling of the Leech River Complex followed Walker Creek magmatism. By ca. 45 Ma, muscovite from one of the Walker Creek intrusions had cooled to ~400 °C. By ca. 42.5 Ma, biotite from nearby pelitic schist had cooled to ~330 °C (Fig. 16B). These temperatures may reflect, in part, static cooling of the Complex following cessation of magmatism. However, the rapid decrease in temperature could be linked to exhumation, arguably during a tectonic event. A simple explanation for exhumation is underthrusting of the Metchosin Igneous Complex beneath the Leech River Complex along the Leech River fault (Clowes et al., 1987; Massey, 1986). This fault is exposed as an anastomosing chloritic mylonite zone, with sinistral-oblique sense of displacement, along the contact between the Metchosin and Leech River complexes (Fairchild, 1979; Muller, 1983; Massey, 1986; Groome, 2000). The Leech River Complex was uplifted, denuded, and exposed at the surface by 35 Ma when it was overlain by sediments of the Oligocene Carmanah Group (Fairchild and Cowan, 1982).

THE ROLE OF SLAB WINDOWS

Ridge subduction and slab window formation provide a compelling cause for magmatism in the Leech River Complex because of (1) the inferred forearc position of the Leech River Complex in Cretaceous to Paleogene time, (2) the peraluminous character of the Jordan River and Walker Creek intrusive suites, and (3) the MORB-like composition of the Tripp Creek metabasite. Taken together, these features are compatible with migration of oceanic spreading ridges beneath the Leech River forearc, leading to high heat flow and the injection of MORB-type magmas into the forearc, and concurrent anatexis of the forearc sedimentary and metasedimentary rocks. Known as the "blowtorch" effect (Delong et al., 1979), this model of ridge-induced melting in the forearc is compatible with early models of ridge subduction (e.g., Uyeda and Miyashiro, 1974; Marshak and Karig, 1977), subsequent structural and magmatic models of slab windows (Dickinson and Snyder, 1979; Thorkelson, 1996), and studies of specific Late Cenozoic near-trench igneous complexes in Chile (Kaeding et al., 1990), the Solomon arc (Johnson et al., 1987), California and Mexico (Johnson and O'Neil, 1984; Rogers and Saunders, 1989), Japan (Hibbard and Karig, 1990), and Vancouver Island (Armstrong et al., 1985).

Walker Creek magmatism in the Leech River Complex lies at the southeastern end of a diachronous belt of forearc intrusions and hydrothermal veins that range in age from ca. 61 Ma in southern Alaska to ca. 50 Ma in southeastern Alaska, and apparently record southward migration of the Kula-Farallon ridge along the continental margin (Haeussler et al., 1995). Although the actual history of triple junction migration may have been complex (Sisson and Pavlis, 1993) and complicated by forearc dismemberment and dextral translation (Smart et al., 1996), the overall southward migration apparently ended at or near the Leech River Complex with the emplacement of the Walker Creek intrusions at ca. 51 Ma.

The absence of significant post–Middle Eocene northward translation of the Pacific Rim and Crescent Terranes, as documented in paleomagnetic studies (Irving and Brandon, 1990; Babcock et al., 1992), implies that the present position of the Leech River Complex is close to where it lay at the time of Walker Creek magmatism, in the Middle Eocene. In contrast, paleomagnetic studies on Eocene rocks from southeastern Alaska indicate large dextral displacements (1400 ± 350 km [13 ± 9°]) from the south (Bol et al., 1992), leaving the position of these rocks uncertain at the time of forearc magmatism. Therefore, the Walker Creek intrusions in the Leech River Complex and the broadly coeval Flores volcanics of the Pacific Rim Complex and the Mount Washington and Clayoquot intrusions on Vancouver Island (Massey, 1995) appear to provide the most accurate location of the Kula–Farallon–North America triple junction in early Middle Eocene time (Fig. 17). This position, along Vancouver Island, was predicted by Thorkelson and Taylor (1989) largely on the basis of chemical variations in the Kamloops-Challis arc in south-central British Columbia and the northwestern United States. Geochemical compilation and tectonic modeling by Breitsprecher and Thorkelson (2001) supports the hypothesis that a slab window formed beneath the Pacific Northwest, with the triple junction located off the coast of present-day Vancouver Island at the time of Walker Creek magmatism.

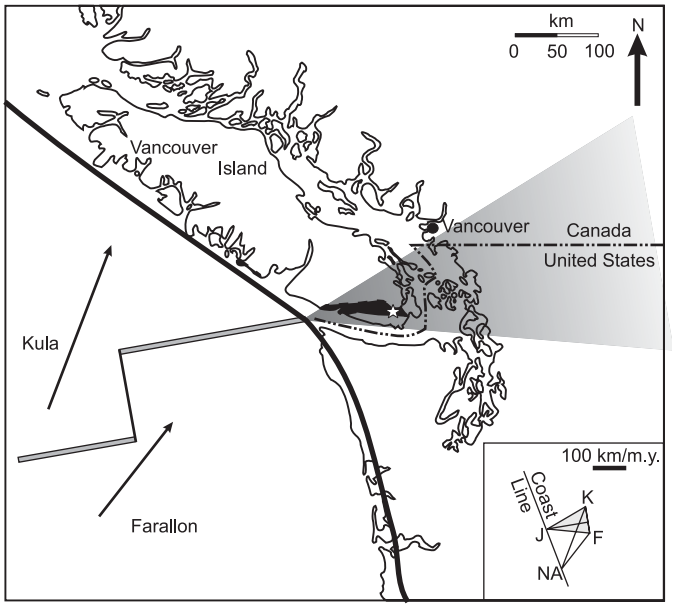

Figure 17. Slab window model for the forearc magmatism in the Leech River Complex at 51 Ma. The Pacific Rim Terrane is indicated by the black shading, and the study area location is indicated by the white star. The heavy dark line represents the inferred location of the North American plate margin in the early Eocene (modified from Dickinson, 1991). Inset: Vector diagram for the Kula (K) and Farallon (F) plates with a fixed North America (NA). J is the position of the triple junction. The shaded region represents the shape of the slab window beneath the North American plate. J-NA vector represents the migration path of the K-F-NA triple junction along the coastline. The orientation of the coastline is taken to be 340°, approximately what it is currently. Vectors are from Babcock et al. (1992) and the principles are from Thorkelson (1996).

CONCLUSIONS

Based on the data and interpretations presented here, a Cretaceous through Eocene history can be deduced for the Leech River Complex. The earliest event in the Leech River Complex's evolution was the deposition of the protolith sediments in a narrow time window in the latest Early Cretaceous and the earliest Late Cretaceous. The timing of sedimentation is constrained between 103 Ma, the age of the youngest detrital zircon in the metasediment, and 88 Ma, the age of Jordan River magmatism.

Between the time of deposition and the time of Jordan River magmatism, the Leech River Complex underwent rapid burial to a depth of approximately 10 km, which is the depth indicated by the metamorphic assemblage in the aureole around the Jordan River metagranodiorite. The speed of this burial, a minimum of 0.6 km/m.y., is indicative of an active tectonic setting. After the burial, it is inferred that the Leech River Complex remained at approximately 10 km depth from the Late Cretaceous through the Middle Eocene. While no direct constraints were found to be dated between 88 Ma and 51 Ma, it can be inferred that the Complex remained at the same *P-T* conditions because the contact metamorphic aureole associated with the Walker Creek intrusions records the same conditions as that around the Jordan River metagranodiorite. The Walker Creek intrusions were dated to be ca. 51 Ma.

After the Walker Creek magmatism, the Leech River Complex underwent rapid exhumation, indicated by the $^{40}Ar/^{39}Ar$ ages from the Leech River Schist. Age determinations on muscovite and biotite indicate that the Leech River Complex underwent rapid cooling shortly after Walker Creek magmatism. Assuming exhumation along the kyanite geotherm, the Complex was exhumed at a minimum rate of 0.8 km/m.y. between ca. 51 Ma and 42.5 Ma, the $^{40}Ar/^{39}Ar$ age from biotite in the schist. The timing of the final exhumation of the Leech River Complex is constrained by the presence of Early Oligocene sedimentary overlap assemblages. For these sediments to be deposited over the Leech River Complex, the Complex must have been completely exhumed. These sediments overlap both the Leech River Complex and Wrangellia, indicating that the Leech River Complex was in its current position relative to Wrangellia by the Early Oligocene.

The timing of these events can be used to constrain the offshore plate configurations along the western margin of North America. The Walker Creek intrusions are interpreted to have formed as a result of the subduction of the Kula-Farallon ridge. Based on paleomagnetic studies of the Eocene Flores Volcanics on Vancouver Island, which indicate that Vancouver Island was in its current location by the Eocene (Irving and Brandon, 1990), the Walker Creek intrusions provide the location of the Kula–Farallon–North America triple junction at ca. 51 Ma.

ACKNOWLEDGMENTS

Funding for this project was provided by Natural Sciences and Engineering Research Council of Canada (NSERC) research grants to DJT and JKM. We would like to thank the critical reviews by Jinny Sisson, Margaret Rusmore and Susan DeBari for insightful and helpful comments and suggestions.

REFERENCES CITED

Armstrong, R.L., Muller, J.E., Harakal, J.E., and Muehlenbachs, K., 1985, The Neogene Alert Bay volcanic belt of northern Vancouver Island, Canada: Descending-plate-edge volcanism in the arc-trench gap: Journal of Volcanology and Geothermal Research, v. 26, p. 75–97.

Babcock, R.S., Burmester, R.F., Engebretson, D.C., and Warnock, A., 1992, A rifted margin for the Crescent basalts and related rocks in the northern Coast Range volcanic province, Washington and British Columbia: Journal of Geophysical Research, v. 97, p. 6799–6821.

Barker, F., Farmer, G.L., Ayuso, R.A., Plafker, G., and Lull, J.S., 1992, The 50 Ma granodiorite of the eastern Gulf of Alaska; melting in an accretionary prism in the forearc: Journal of Geophysical Research, v. 97, p. 6757–6778.

Best, M.G., 1982, Igneous and metamorphic petrology: New York, W.H. Freeman and Company, 630 p.

Bol, A.J., Coe, R.S., Gromme, C.S., and Hillhouse, J.W., 1992, Paleomagnetism of the Resurrection Peninsula, Alaska; implications for the tectonics of southern Alaska and the Kula-Farallon Ridge: Journal of Geophysical Research, v. 97, p. 17,213–17,232.

Brandon, M.T., 1989, Deformational styles in a sequence of olistostromal melanges, Pacific Rim Complex, western Vancouver Island, Canada: Geological Society of America Bulletin, v. 101, p. 1520–1542.

Brandon, M.T., Cowan, D.S., and Vance, J.A., 1988, The Late Cretaceous San Juan thrust system, San Juan Islands, Washington: Boulder, Colorado, Geological Society of America Special Paper 221, 81 p.

Breitsprecher, K., and Thorkelson, D.J., 2001, Spatial coincidence of the Kula-Farallon slab window with trench-distal volcanism of the Eocene Magmatic Belt in the southern Cordillera, *in* Cook, F., and Erdmer, P., compilers, Slave-Northern Cordillera Lithospheric Evolution (SNORCLE) Transect and Cordilleran Tectonics Workshop Meeting (February 22–25), Pacific Geoscience Centre: Lithoprobe Report No. 79, p. 178–182.

Bucher, K and Frey, M., 1994, Petrogenesis of metamorphic rocks (6th edition): Complete revision of Winkler's textbook: Berlin, Springer Verlag, 318 p.

Clowes, R.M., Brandon, M.T., Green, A.G., Yorath, C.J., Sutherland Brown, A., Kanasewich, E.R., and Spencer, C., 1987, LITHOPROBE—Southern Vancouver Island: Cenozoic subduction complex imaged by deep seismic reflections: Canadian Journal of Earth Sciences, v. 24, p. 31–51.

Debari, S.M., Anderson, R.G., and Mortensen, J.K., 1999, Correlations among lower to upper crustal components in an island arc: The Jurassic Bonanza arc, Vancouver Island, Canada: Canadian Journal of Earth Sciences, v. 36, p. 1371–1413.

DeLong, S.E., Schwarz, W.M., and Anderson, R.N., 1979, Thermal effects of ridge subduction: Earth and Planetary Science Letters, v. 44, p. 239–246.

Dickinson, W.R., 1991, Tectonic setting of faulted Tertiary strata associated with the Catalina core complex in southern Arizona: Boulder, Colorado, Geological Society of America Special Paper 264, 106 p.

Dickinson, W.R., and Snyder, W.S., 1979, Geometry of triple junctions related to San Andreas transform: Journal of Geophysical Research, v. 84, p. 561–572.

Duncan, R.A., 1982, A captured island chain in the Coast Range of Oregon and Washington: Journal of Geophysical Research, v. 87, p. 10,827–10,837.

Fairchild, L.H., 1979, The Leech River unit and Leech River fault, southern Vancouver Island, British Columbia [M.S. thesis]: Seattle, University of Washington, 170 p.

Fairchild, L.H., and Cowan, D.S., 1982, Structure, petrology, and tectonic history of the Leech River Complex northwest of Victoria, Vancouver Island: Canadian Journal of Earth Sciences, v. 19, p. 1817–1835.

Forsythe, R.D., and Nelson, E.P., 1985, Geological manifestations of ridge collision: Evidence from the Golfo de Penas-Taitao Basin, southern Chile: Tectonics, v. 4, p. 477–495.

Friedman, R.M., and Armstrong, R.L., 1995, Jurassic and Cretaceous U-Pb geochronometry of the southern Coast Belt, British Columbia, 49°–51° N, *in* Miller, D.M., and Busby, C., eds., Jurassic magmatism and tectonics of the North American Cordillera: Boulder, Colorado, Geological Society of America Special Paper 299, p. 95–139.

Frost, B.R., Chamberlain, K.R., and Schumacher, J.C., 2000, Sphene (titanite); phase relations and role as a geochronometer: Chemical Geology, v. 172, p. 131–148.

Gehrels, G.E., Dickinson, W.R., Ross, G.M., Stewart, J.H., and Howell, D.G., 1995, Detrital zircon reference for Cambrian to Triassic miogeoclinal strata of western North America: Geology, v. 23, p. 831–834.

Gill, J.B., 1981, Orogenic andesites and plate tectonics: Berlin, Springer, 390 p.

Groome, W.G., 2000, Magmatism and metamorphism in the Leech River Complex, southern Vancouver Island, British Columbia, Canada—Implications for Eocene tectonics of the Pacific Northwest [M.S. thesis]: Burnaby, British Columbia, Simon Fraser University, 220 p.

Groome, W.G., Friedman, R.M., Massey, N.W.D., Thorkelson, D.J., Layer, P.W., and Marshall, D., 1999, Evidence from the Leech River Complex for Eocene deformation and accretion on southern Vancouver Island, British Columbia, *in* Evenchick, C.A., et al., eds., Terrane paths '99: Circum-Pacific Terrane Conference, Okanagan Valley, B.C., Canada, September 26–October 1, 1999, Abstracts and Program, p. 39.

Groome, W.G., Thorkelson, D.J., Friedman, R.M., Massey, N.W.D., and Marshall, D.D., 2000, Eocene magmatism in the Leech River Complex: Evidence for spreading ridge subduction and slab window formation: Geological Society of America Abstracts with Programs, v. 32, no. 6, p. A-15.

Haeussler, P.J., Bradley, D., Goldfarb, R., Snee, L., and Taylor, C., 1995, Link between ridge subduction and gold mineralization in southern Alaska: Geology, v. 23, p. 995–998.

Halliday, A.N., Fallick, A.E., Dickin, A.P., Mackenzie, A.B., Stephens, W.E., and Hildreth, W., 1983, The isotopic and chemical evolution of Mount St. Helens: Earth and Planetary Science Letters, v. 63, p. 241–256.

Harris, N.R., Sisson, V.B., Wright, J.E., and Pavlis, T.L., 1996, Evidence for Eocene mafic underplating during forearc intrusive activity, eastern Chugach Mountains, Alaska: Geology, v. 24, p. 263–266.

Hibbard, J.P., and Karig, D.E., 1990, Structural and magmatic responses to spreading ridge subduction: An example from southwest Japan: Tectonics, v. 9, p. 207–230.

Hill, M., Morris, J., and Whelan, J., 1981, Hybrid granodiorites intruding the accretionary prism, Kodiak, Shumagin, and Sanak Islands, southwest Alaska: Journal of Geophysical Research, v. 86, p. 10,569–10,590.

Irving, E., and Brandon, M.T., 1990, Paleomagnetism of the Flores Volcanics, Vancouver Island, in place by Eocene time: Canadian Journal of Earth Sciences, v. 27, p. 811–817.

Johnson, C.M., and O'Neil, J.R., 1984, Triple junction magmatism: A geochemical study of Neogene volcanic rocks in western California: Earth and Planetary Science Letters, v. 71, p. 241–262.

Johnson, R.W., Jaques, A.L., Langmuir, C.H., Perfit, M.R., McColloch, M.T., Staudigel, H., Chapell, B.W., and Taylor, S.R., 1987, Ridge subduction and forearc volcanism: Petrology and geochemistry of rocks dredged from the western Solomon arc and Woodlark Basin, *in* Taylor, B., and Exon, N., eds., Marine geology, geophysics and geochemistry of the Woodlark Basin, Solomon Islands: Houston, Texas, Circum-Pacific Council for Energy and Mineral Resources, Earth Science Series, v. 7, p. 113–154.

Johnston, S.T., and Thorkelson, D.J., 1997, Cocos-Nazca slab window beneath Central America: Earth and Planetary Science Letters, v. 146, p. 465–474.

Journeay, J.M., and Friedman, R.M., 1993, The Coast Belt thrust system: Evidence of Late Cretaceous shortening in southwest British Columbia: Tectonics, v. 12, p. 756–775.

Kaeding, M., Forsythe, R.D., and Nelson, E.P., 1990, Geochemistry of the Taitao ophiolite and near-trench intrusions from the Chile margin triple junction: Journal of South American Earth Sciences, v. 3, p. 161–177.

Kirschner, D.L., Hunziker, J.C., and Cosca, M., 1996, Closure temperature of argon in micas; a review and reevaluation based on Alpine samples: Geological Society of America Abstracts with Programs, v. 28, no. 7, p. 441.

Marshak, R.S., and Karig, D.E., 1977, Triple junctions as a cause for anomalously near-trench igneous activity between the trench and volcanic arc: Geology, v. 5, p. 233–236.

Massey, N.W.D., 1986, Metchosin Igneous Complex, southern Vancouver Island: Ophiolite stratigraphy developed in an emergent island setting: Geology, v. 14, p. 602–605.

Massey, N.W.D., 1995, Geology and mineral resources of the Alberni–Nanaimo Lakes sheet, Vancouver Island 92F/1W, 92F/2E and part of 92F/7E: British Columbia Ministry of Energy, Mines and Petroleum Resources, Geological Survey Branch, Paper 1992-2, 132 p.

Muller, J.E., 1983, Geology, Victoria map area: Geological Survey of Canada Map 1553A, scale 1:100,000.

Paterson, S.R., and Fowler, T.K., 1993, Re-examining pluton emplacement processes: Journal of Structural Geology, v. 15, p. 191–206.

Pearce, J.A., Harris, N.B.W., and Tindle, A.G., 1984, Trace element discrimination diagrams for the tectonic interpretation of granitic rocks: Journal of Petrology, v. 25, p. 956–983.

Read, P.B., Woodsworth, G.J., Greenwood, H.J., Ghent, E.D., and Evenchick, C.A., 1991, Metamorphic map of the Canadian Cordillera: Geological Survey of Canada Map 1714A, scale 1:2,000,000.

Rogers, G., and Saunders, A.D., 1989, Magnesian andesites from Mexico, Chile, and the Aleutian Islands: Implications for magmatism associated with ridge-trench collisions, *in* Crawford, A.J., ed., Boninites and related rocks: London, Unwin Hyman, p. 416–445.

Ross, G.M., and Parrish, R.R., 1991, Detrital zircon geochronology of metasedimentary rocks in the southern Omenica Belt, Canadian Cordillera: Canadian Journal of Earth Sciences, v. 28, p. 1254–1270.

Rubin, C.M., Saleeby, J.B., Cowan, D.S., Brandon, M.T., and McGroder, M.F., 1990, Regionally extensive mid-Cretaceous west-vergent thrust system in the northwestern Cordillera; implications for continent-margin tectonism: Geology, v. 18, p. 276–280.

Rusmore, M.E., 1982, Structure and petrology of pre-Tertiary rocks near Port Renfrew, Vancouver Island, British Columbia [M.S. thesis]: Seattle, University of Washington, 24 p.

Rusmore, M.E., and Cowan, D.S., 1985, Jurassic-Cretaceous rock units along the southern edge of the Wrangellia Terrane on Vancouver Island: Canadian Journal of Earth Sciences, v. 22, p. 1223–1232.

Shouldice, D.H., 1971, Geology of the Western Canadian Continental Shelf: Bulletin of Canadian Petroleum Geology, Canadian Society of Petroleum Geologists, v. 19, p. 405–436.

Sisson, V.B., and Pavlis, T.L., 1993, Geologic consequences of plate reorganization: An example from the Eocene southern Alaska forearc: Geology, v. 21, p. 913–916.

Smart, K.J., Pavlis, T.L., Sisson, V.B., Roeske, S.M., and Snee, L.W., 1996, The Border Ranges fault system in Glacier Bay National Park, Alaska; evidence for major early Cenozoic dextral strike-slip motion: Canadian Journal of Earth Sciences, v. 33, p. 1268–1282.

Sun, S.-S., and McDonough, W.F., 1989, Chemical and isotopic systematics of oceanic basalts: Implications for mantle compositions and processes, *in* Saunders, A.D., and Norry, M.J., eds., Magmatism in the ocean basins: Geological Society [London] Special Publication No. 42, p. 313–345.

Thorkelson, D.J., 1996, Subduction of diverging plates and the principles of slab window formation: Tectonophysics, v. 255, p. 47–63.

Thorkelson, D.J., and Taylor, R.P., 1989, Cordilleran slab windows: Geology, p. 17, p. 833–836.

Uyeda, S., and Miyashiro, A., 1974, Plate tectonics and the Japanese Islands: A synthesis: Geological Society of America Bulletin, v. 85, p. 1159–1170.

Wells, R.E., Engebretson, D.C., Snavely Jr., P.D., and Coe, R.S., 1984, Cenozoic plate motions and the volcano-tectonic evolution of western Oregon and Washington (USA): Tectonics, v. 3, p. 275–294.

Wheeler, J.O., and McFeeley, P., compilers, 1991, Tectonic assemblage map of the Canadian Cordillera and adjacent parts of the United States of America: Geological Survey of Canada Map 1712A, scale 1:2,000,000.

Manuscript Accepted by the Society February 5, 2003

Printed in the USA